

1 **SM-Omics: An automated platform for high-throughput spatial**
2 **multi-omics**

3 Sanja Vickovic^{1,*,#}, Britta Lötstedt^{1,2,*}, Johanna Klughammer¹, Åsa Segerstolpe¹, Orit
4 Rozenblatt-Rosen¹, Aviv Regev^{1,3,4,#}

5
6 ¹Klarman Cell Observatory Broad Institute of MIT and Harvard, Cambridge, MA, USA.

7 ²Science for Life Laboratory, Department of Gene Technology, KTH Royal Institute of
8 Technology, Stockholm, Sweden.

9 ³Howard Hughes Medical Institute and Koch Institute for Integrative Cancer Research,
10 Department of Biology, Massachusetts Institute of Technology, Cambridge, MA, USA.

11 ⁴Current address: Genentech, 1 DNA Way, South San Francisco, CA, USA.

12
13

14 *These authors contributed equally to this work

15 # To whom correspondence should be addressed: vickovic@broadinstitute.org (S.V.),
16 aregev@broadinstitute.org (A.R.)

17 **Abstract**

18

19 The spatial organization of cells and molecules plays a key role in tissue function in
20 homeostasis and disease. Spatial Transcriptomics (ST) has recently emerged as a key technique to
21 capture and positionally barcode RNAs directly in tissues. Here, we advance the application of ST
22 at scale, by presenting Spatial Multiomics (SM-Omics) as a fully automated high-throughput
23 platform for combined and spatially resolved transcriptomics and antibody-based proteomics.

24 Introduction

25
26 The spatial organization of cells and molecules is fundamental to physiological function
27 and disease pathology, and imaging the position and level of molecules is a cornerstone of both
28 basic biology and clinical pathology. Because gene expression is regulated at multiple levels from
29 transcription to protein degradation, protein and RNA levels convey distinct information on gene
30 function and cell state, as has been shown in diverse contexts including dynamic responses[1,2],
31 in genetic variation[3], in human malignancies[4], and in single cells in suspension[5]. Single cell
32 genomics and multi-omics approaches, such as single cell and single nucleus RNA-Seq[6–11] and
33 CITE-Seq[5,12], have been tremendously successful at profiling diverse molecular profiles at the
34 level of individual cells and nuclei, but typically do not preserve spatial information. The
35 importance of studying cells in their native environment has been shown in many processes, from
36 normal organ development to spatial deregulation in diseases and often highlighted in the context
37 of cancer propagation and resistance to therapy[13,14].
38

39 Recent progress in spatial *in situ* profiling methods has opened the way for comprehensive
40 profiling of location and expression simultaneously[15–27]. For spatial RNA measurements,
41 Spatial Transcriptomics (ST)[24,26] has emerged as a versatile approach for spatial RNA
42 profiling. In ST, a fresh-frozen tissue section is placed on top of barcoded DNA primers attached
43 to a glass surface[24]. Following tissue staining and histological imaging, cells are permeabilized,
44 mRNAs are spatially tagged directly in tissues and a cDNA sequencing library is generated. After
45 sequencing, the RNA-Seq information is traced back to the spatially barcoded positions on the
46 glass slide providing a global spatial tissue profile. ST has been applied to diverse systems and
47 tissue types, such as brain, heart, spinal cord, melanomas, breast cancer and prostate cancer[24,28–
48 35]. However, barriers around throughput, resolution, and efficiency[36], limit its application at
49 large scale. In parallel, there have been advances in multiplex protein measurements *in situ* based
50 on reading out multiple fluorescent-, heavy metal- or barcode coupled antibody tags at a
51 time[19,20,37–40]. Some methods rely on cyclic immunostaining or *in situ* sequencing barcoding
52 schemes, whereas others use expensive machinery for Multiplexed Ion Beam Imaging or Imaging
53 Mass Cytometry. Few methods have combined RNA and antibody-based measurements[41,42]
54

55 To bridge this gap and make molecular tissue profiling a widely available and robust tool,
56 we have developed Spatial Multi-Omics (SM-Omics), an end-to-end framework that uses a liquid
57 handling platform for high-throughput combined transcriptome and antibody-based spatial tissue
58 profiling with minimum user input and available laboratory instrumentation[43,44]. SM-Omics
59 allows processing of up to 96 sequencing-ready libraries, of high complexity, in a ~2 days, making
60 it the first truly high-throughput platform for spatial multi-omics.
61

62 Results and Discussion

63
64 We devised SM-Omics for high throughput combined transcriptomics and antibody-based
65 measurements. SM-Omics can be used for either Spatial Transcriptomics alone, or, in combination
66 with fluorescently or DNA-barcoded antibodies to simultaneously measure spatial profiles of
67 RNAs and proteins. Briefly, in SM-Omics, after tissue staining for traditional histology (H&E),

68 immunofluorescence or using DNA-barcoded antibodies, glass slides are loaded into the SM-
69 Omics platform, where, using a liquid handler robot, cells are permeabilized, mRNAs and/or
70 antibody barcodes are spatially tagged and converted into a sequencing-ready library (**Fig1a**). The
71 process consists of three main parts with designed stopping points to either store the processed
72 material or load required reagents for the upcoming reactions. The first step consists of all *in situ*
73 enzymatic reactions on the SM-Omics slide, including tissue permeabilization after staining and
74 reverse transcription with simultaneous release of spatial capture probes (**Fig1a, I**). Each such *in*
75 *situ* run holds up to 4 slides with tissues, with the number of active areas with spatial probes per
76 slide ranging from one to 16 per slide. The second and third steps consist of RNA-Seq library
77 preparation in standard 96 well plates, where the user can choose to run between 1 and 96 samples
78 in parallel in 8-step increments with adjusted library consumable usage to alleviate costs. The input
79 to these is *in situ* tissue cDNA or antibody tag material collected from SM-Omics slides in the first
80 step, which are then processed to amplify cDNA using a T7 *in vitro* transcription approach (for
81 cDNA) or standard PCR amplification (for antibody tags), followed by a final conversion of the
82 amplified RNAs into sequencing-ready libraries (**Fig1a, II-III**).

83
84 SM-Omics introduces four key enhancements compared to ST: (1) Automation, requiring
85 minimal user intervention; (2) throughput, allowing processing of 96 samples in a 2-day cycle; (3)
86 enhanced quality, reflected by higher complexity RNA-Seq libraries and (4) combining RNA-Seq
87 measurements with proteomics measurements including immunofluorescent (IF) staining and
88 antibody-barcoding strategies. We first describe the core approach in the context of spatial RNA
89 measurements (**Fig1a, II-III**), and then its extension to include spatial protein measurements.

90
91 To test the performance of SM-Omics for spatial transcriptomics, we assessed the
92 feasibility, reproducibility and efficiency of RNA data in two key steps, testing on the mouse
93 olfactory bulb (MOB) and mouse cortex: (1) *in situ* tissue reactions (cDNA capture) and (2) library
94 (RNA-Seq) preparation.

95
96 SM-Omics had enhanced performance in terms of *in situ* reactions compared to standard
97 ST, with minimal lateral diffusion and comparable and reproducible cDNA signal intensity.
98 Specifically, we first ran *in situ* reactions on the glass surface in optimization mode, where cDNA
99 molecules are *in situ* fluorescently labeled to create a spatial cDNA footprint[35] (**FigS1a**). We
100 compared the localized cDNA footprint to the histological H&E pattern and measured the lateral
101 tissue permeabilization effects. This provides an optimal set of parameters needed to successfully
102 run tissue-specific reactions and to ensure minimal lateral cross-talk between adjacent spatial
103 measurements. Testing on the adult mouse cortex (**FigS1b-e**) showed that SM-Omics resulted in
104 no mixing of material between spatial measurements with no lateral diffusion (mean $-0.06 \mu\text{m} \pm$
105 0.51 sd), which is 4X weaker lateral diffusion signal than in ST performed on adjacent tissue
106 sections ($p < 0.01$, two-sided *t*-test, **FigS1f,g**), and 30x weaker diffusion signal compared to
107 previous reports[24,35,45]. Moreover, the signal intensity of the fluorescent cDNA footprint was
108 highly reproducible within and between SM-Omics runs: there were no significant differences
109 (Wilcoxon rank-sum test, $p > 0.05$) between the cDNA signal intensities from adjacent adult mouse
110 main olfactory bulb (MOB) tissue replicates on a single glass slide ($n=3$), single run ($n=3$) or
111 separate runs ($n=3$) (**FigS2**). SM-Omics yielded robust spatial fluorescent patterns in three other
112 tissues: mouse cortex, a mouse model of colorectal cancer, and a distal part of the mouse colon
113 (**FigS3**).

114
115 To process the generated data efficiently, we also developed SpoTteR, a fast and fully
116 automated end-to-end image integration method. With SpoTteR, images are automatically
117 downscaled and barcode spots positions reconstructed using iterative blob detection and grid
118 fitting (**Methods**), accounting for common imaging artifacts, such as uneven tissue coloration or
119 pipetting bubbles. SpoTteR then registers tissue coordinates through a masking process to produce
120 a gene-by-barcode matrix overlaid on top of morphological features (**FigS4**). Compared to manual
121 and semi-automated approaches[46] SpoTter is up to 14X faster with low false discovery rates (FP
122 3.54% and FN 1.18%, vs. >15% of grid spots as FNs in other approaches[46]; **FigS5**), when
123 applied to human lung cancer, human arthritis and mouse colon data.

124
125 Using the SM-Omics end-to-end toolbox (**Fig1a**) we prepared and sequenced 18 SM-
126 Omics libraries from the main olfactory bulb of the adult mouse brain, and compared them to
127 standard ST libraries. SM-Omics libraries were more sensitive than ST, with a 58% higher number
128 of protein-coding genes (4,369 genes), and 1.5-fold higher number of unique transcripts (UMIs)
129 (Wilcoxon's rank-sum test, $p \leq 0.05$, **Methods, FigS6a,b**). Both ST and SM-Omics had similar
130 correlations between their respective pseudo-bulk averages and replicates (**FigS6c**), but SM-
131 Omics exhibited an increase on average ($n=3$) in the number of transcripts captured in more than
132 half of the annotated morphological regions (**Methods, FigS6d**). SM-Omics ($n=3$) also
133 performed comparably to newer generation array designs ($n=3$) (Visium,
134 10X Genomics) in detected genes and UMIs per measurement ($p \geq 0.05$,
135 Wilcoxon's rank sum test) in the adult mouse brain cortex tissues
136 (**FigS6e-g**). We also confirmed that our liquid handling system processed
137 standard spatial library preparations robustly with no significant
138 variation (Wilcoxon's rank-sum test, $p \geq 0.05$) between runs (**FigS7a-b**). This
139 increased efficiency in SM-Omics, as reflected in the number of genes and UMIs detected per (x,y)
140 coordinate, was due to several optimizations in library preparations. First, we introduced
141 simultaneous release of barcoded primers and capture of mRNA molecules (**Methods**). This
142 hybrid can then be used as a template in the reverse transcription reaction in solution instead of
143 solid surface as previously performed; this also decreased total processing time from ~1.5 days to
144 ~6h. Second, we improved the efficiency of library preparation reactions, by increasing
145 the amount of sequencing adaptors and reaction time for adaptor
146 ligation to the template (Wilcoxon's rank sum test, $p \leq 0.05$) (**FigS7c-d**).

147
148 We also compared SM-Omics and ST in terms of specific detection of known and novel
149 specific spatial expression patterns. We used Splotch[31,47] to align our replicate tissue sections
150 and generate posterior spatial gene expression estimates. We confirmed that region-enriched and
151 upregulated genes were present in the major spatial layers (**Methods**) of the MOB compared to
152 the Allen Brain Atlas[48] (**FigS8a,b**). While known gene patterns detected as layer-enriched
153 agreed between SM-Omics and ST (**FigS8c-f**), SM-Omics's overall specificity was higher
154 (**FigS8a**). The increased sensitivity at the same sequencing depth (by down-sampling, **Methods**),
155 allowed us to reproducibly measure the spatial gene expression of newly detected targets, such as
156 *Ctgf* in the Glomerular Layer, *Camk4* in the Granular Cell Layer, *Lancl3* in the Mitral Layer and
157 *Cbln4* in the Outer Plexiform Layer (**Fig1b,c**).

158

159 Next, we implemented a combined spatial transcriptomics and antibody-based read-out
160 into our fully automated spatial multi-omics platform, by using either immunofluorescence and
161 imaging or DNA-barcoding and sequencing.

162
163 We first developed a protocol that combined antibody-based immunofluorescence (IF)
164 with spatial transcriptomics (**Fig2a, Methods**). Localized cDNA footprints after nuclear (DAPI)
165 and IF stainings of the tissue (**Fig2b, FigS9a**) showed that mRNAs were laterally diffusing only
166 $0.16 \pm 1.21 \mu\text{m}$ outside of the nucleus, again indicating minimal lateral cross-talk between adjacent
167 spatial measurements. We next created SM-Omics mouse brain cortex libraries following
168 immunostaining with an antibody against the brain protein NeuN, which is highly expressed in
169 most neuron nuclei (**Fig2c**). Library complexities, signal specificity and RNA expression patterns
170 were similar to those in standard (H&E stained) ST measurements and in the Allen Brain Atlas[48]
171 (**FigS9b-d**), confirming that our protocol for simultaneous immunofluorescent and transcriptome
172 measurements provided high-quality mRNA data. Next, comparing the antibody IF signals and
173 corresponding RNA expression (**Fig2c**), there was significant correlation between NeuN mRNA
174 and protein expression (Spearman's ρ 0.73, **p-value** ≤ 0.05 , **Fig2c**). Notably, in some regions
175 (*e.g.*, hypothalamus) RNA expression was low but protein expression was substantial (**Fig2c**). This
176 may be due to either a biological difference, or to the differences in sensitivity and saturation of
177 RNA-Seq *vs.* IF.

178
179 Finally, we introduced an antibody DNA-barcoding system[5] compatible with spatial
180 transcriptomics to increase multiplexing capacities otherwise limited with spectral overlap in
181 imaging approaches (**Fig3a**). We tag each of 6 antibodies[5] with an amplification primer and an
182 individual barcode tag followed by a poly(d)A sequence for capture on a poly(d)T spatially
183 barcoded array (**Methods**). We used a similar tissue staining protocol as that for
184 immunofluorescence, where the tissue was first *in situ* fixed with paraformaldehyde to ensure
185 specific antigen coupling, followed by antibody staining, tissue permeabilization and SM-Omics
186 library preparation (**Fig3a**). To benchmark our approach, we incubated adult mouse spleen tissue
187 sections with both a fluorescently labeled antibody and a barcoded antibody, allowing us to
188 simultaneously validate and directly compare both detection methods. We imaged the
189 fluorescently labeled epitopes prior to any *in situ* enzymatic reactions on the array surface, coupled
190 the antibody tags to the spatial array, such that they were copied into a stable covalent complex,
191 while mRNA was spatially captured and transcribed on the array (**Fig3a**). We first tested a two-
192 antibody cocktail targeting F4/80 (staining splenic red pulp macrophages) and IgD (staining
193 marginal zone B cells in the white pulp) (**Fig3b**). We obtained high quality antibody tag (mean \pm sd
194 142 ± 15 UMIs per SM-Omics measurement; $n=3$) and cDNA libraries ($1,375 \pm 181$ UMIs per SM-
195 Omics measurement, $n=3$), with highly specific antibody tag patterns (**Fig3b**) that were well-
196 correlated to the corresponding IF intensities across all major splenic regions (**FigS10a**, on average
197 78%). RNA and antibody tag levels were in agreement for IgD (Spearman's $\rho = 0.74$, **p-**
198 **value** ≤ 0.05 across all spatial measurements), and less so for F4/80 (Spearman's $\rho = 0.65$, **p-**
199 **value** ≤ 0.05 across all spatial measurements) (**FigS10b**). Finally, an SM-Omics experiment
200 with 6 validated[49] barcoded antibodies targeting F4/80, IgD, CD163, CD38, CD4, and CD8a
201 (**FigS10c**) successfully combined spatial transcriptomics and protein estimates in a highly
202 multiplexed manner (**Fig3c**). CD4 and CD8 proteins (by antibody signal) and their corresponding
203 mRNAs were spatially localized in the PALS zone, whereas IgD and CD38 protein and mRNA
204 were enriched in the B follicles. F4/80 protein and mRNA were localized to the red pulp, but the

205 corresponding mRNA (*Adgre1*) was also enriched in the marginal zone. Finally, CD163 was
206 differentially expressed, as expected, in the red pulp with Cd163 mRNA also high in PALS.
207

208 **Conclusions**

209
210 SM-Omics is an efficient and automated workflow for combined and spatially resolved
211 transcriptomics and antibody-based proteomics, adaptable to new array versions and designs. SM-
212 Omics provides a more detailed molecular high-plex multi-omics characterization of tissues *in situ*
213 and is the first high-throughput automated system for quantifying the spatial transcriptome and
214 antibody-based proteome, by either immunofluorescence or using DNA barcoded antibodies. We
215 confirmed SM-Omics as a robust system that can reconstruct specific cell associations across
216 morphological layers[50,51], and characterize tissue niches in combination with antibody staining,
217 which provide higher resolution views independently of or in combination with spatial
218 transcriptomics patterns. Its automation on a widely-used platform enables use of appropriate study
219 design while minimizing technical variation, and allowing broad adoption. SM-Omics does not
220 rely on any customized microfabrication, uses commercially, widely-available liquid handlers and
221 reagents with minimum preparation time per run (~30 min), has an end-to-end image-integrated
222 data analysis pipeline and is readily deployable to the wide scientific community.
223

224 **Materials and methods**

225 **Bravo system requirements**

226
227 Bravo Automated Liquid Handling Platform (Agilent Technologies, USA) was equipped
228 with a 96LT pipetting head (G5498B#042, Agilent Technologies, USA) and two Peltier thermal
229 stations (CPAC Ultraflat HT 2-TEC, #7000166A, Agilent Technologies, USA) with PCR adapter
230 having a mounting frame at positions 4 and 6 on the Bravo Deck and connected to an Inheco MTC
231 Controller. On position 7, we recommend the MAGNUM FLX™ Enhanced Universal Magnet
232 Plate (#A000400, Alpaqua, USA) to serve for magnetic bead-based clean ups. In addition, a
233 BenchCel NGS Workstation (Front-load rack at 660 mm height) and BenchCel Configuration
234 Labware MiniHub (option #010, Agilent Technologies, USA) were included in the automation
235 platform setup. In case *in situ* reactions were performed, the PCR adapter was removed from
236 position 6 to be replaced with Aluminum Heat Transfer Plate (#741I6-GS-4, V&P Scientific, Inc,
237 USA).

238

239 **Sample collection and cryosectioning**

240

241 A small piece of freshly collected tissue (~25-50 mg, about 5x5 mm) was placed on a dry
242 and sterile Petri dish, which was placed on top of wet ice. The tissue was then very gently moved
243 using forceps and placed on another dry part of the Petri dish to ensure little liquid was present
244 around the tissue. The bottom of a cryomold (5x5mm, 10x10mm or 25x20mm) was filled with
245 pre-chilled (4°C) OCT (Tissue-Tek; Sakura Finetek, USA) and the tissue transferred with forceps
246 into the OCT-prefilled mold. The entire tissue surface was covered with pre-chilled OCT. The
247 mold was then placed on top of dry ice and allowed the tissue to freeze for up to 5 minutes until

248 OCT has turned completely white and hard. The tissue cryomolds were stored at -80°C until use.
249 For cryosectioning, the ST slide and the tissue molds first reached the temperature of the cryo
250 chamber. The OCT-embedded tissue block was attached onto a chuck with pre-chilled OCT and
251 allowed to freeze ~5-10 min. The chuck was placed in the specimen holder and adjusted the
252 position to enable perpendicular sectioning at 10µm thickness. Sections were gently transferred to
253 a ST array[24] and then the back side of the slide was warmed ~10-15 sec with a finger. ST slides
254 with tissue sections on top could be stored at -80°C for up to 6 days.
255

256 **Tissue fixation and H&E staining**

257
258 The ST slide with the tissue section was warmed to 37°C for 1 minute on a thermal
259 incubator (Eppendorf Thermomixer Option C, Germany). The tissue was then covered with 4%
260 formaldehyde (Sigma-Aldrich, USA) in 1X PBS (Thermo Fisher Scientific, USA) for 10 minutes
261 at room temperature (RT). The whole slide was then washed in 1X PBS in a vertical orientation to
262 be placed back on a horizontal place for drying. 500µl isopropanol covered the tissue and ensured
263 drying. The slide was put into an EasyDip Slide Jar Staining System (Weber Scientific) holder and
264 the same system used for H&E staining. Five ~80 ml containers were prepared with Dako Mayers
265 hematoxylin (Agilent, USA), Dako Bluing buffer (Agilent, USA), 5% Eosin Y (Sigma-Aldrich,
266 USA) in 0.45M Tris acetate (Sigma-Aldrich, USA) buffer at pH 6 and two jars with nuclease-free
267 water (ThermoFisher Scientific, USA). The slide rack was fully immersed in hematoxylin for 6
268 minutes and then washed by dipping the slide rack in a nuclease-free water jar 5 times following
269 another destaining wash by dipping the slide rack in 800mL nuclease-free water for 30 times. The
270 slide rack was put into the Dako bluing buffer and incubated for 1 minute. The slide was again
271 washed by dipping the rack 5 times in the second nuclease-free water jar. The slide rack was finally
272 put into the eosin and incubated for 1 minute to be washed by dipping the rack 7 times in the
273 second water jar. The slide was removed from the rack to allow it to dry.
274

275 **Tissue fixation and IF staining**

276
277 The ST slide with the tissue section was warmed to 37°C for 4 minutes on a thermal
278 incubator (Eppendorf Thermomixer Option C, Germany) and *in situ* fixed and washed as described
279 above. The slide was then mounted in the plastic slide holder (ProPlate Multi-Array slide system;
280 GraceBioLabs, USA) compatible with the Aluminum Heat Transfer Plate (#741I6-GS-4, V&P
281 Scientific, Inc, USA) on position 6 on the Bravo deck. All following antibody incubations were
282 performed at 4°C. First, the tissues were blocked with the TruStain FcX™ PLUS (anti-mouse
283 CD16/32, Biolegend, USA) antibody (1:100 dilution) in 0.5% Triton X-100 (Sigma-Aldrich,
284 USA) for mouse brain tissues and 1% saponin (Sigma-Aldrich, USA) supplemented with 5% FBS
285 (ThermoFisher Scientific, USA) for splenic tissues. This simultaneous blocking and
286 permeabilization step lasted for 30 min. Next, the slide was washed 3x with 1x PBS (ThermoFisher
287 Scientific, USA). After discarding the last wash, the slides were incubated with 1x PBS for 2 min.
288 Then, antibodies were added at 1:100 dilution in 1% saponin (Sigma-Aldrich, USA) supplemented
289 with 5% FBS (ThermoFisher Scientific, USA) for 90 min. The complete list of antibody clones
290 and suppliers is available in **Supplementary Table 1**. The slide was again washed in the same
291 fashion and counterstained with DAPI (Sigma-Aldrich, USA) diluted 1:1000 in 0.5% Triton X-
292 100 (Sigma-Aldrich, USA) for 5 min. In case the reactions were performed on a SM-Omics array

293 and not a mock polyd(T) array, the DAPI reaction was also supplemented with a Cy3 labeled anti-
294 frame DNA probe (5'-Cy3-GGTACAGAAGCGCGATAGCAG-3', IDT, USA) at 10 nM
295 concentration. In case DAPI counterstaining was not used, the step was skipped. This was followed
296 by another wash cycle. The slides were then air dried and mounted with 85% glycerol prior to
297 imaging.
298

299 **Tissue fixation and DAPI-only staining**

300
301 Similarly to performing *Tissue fixation and IF staining*, tissue sections were attached to
302 slides and *in situ* fixed. The slide was then mounted in the plastic slide holder (ProPlate Multi-
303 Array slide system; GraceBioLabs, USA) and all reactions performed at 4°C. Tissues were first
304 incubated with 0.5% Triton X-100 (Sigma-Aldrich, USA) for 25 min. Next, the slide was washed
305 1x PBS (ThermoFisher Scientific, USA) and the tissue stained with DAPI (Sigma-Aldrich, USA)
306 diluted 1:1000 in 0.5% Triton X-100 (Sigma-Aldrich, USA) for 15 min. If the reactions were
307 performed on a SM-Omics array and not a mock polyd(T) array, the DAPI reaction was also
308 supplemented with a Cy3 labeled anti-frame DNA probe (5'-Cy3-
309 GGTACAGAAGCGCGATAGCAG-3', IDT, USA) at 10 nM concentration in order to facilitate
310 image registration to the SM-Omics array coordinates. This was followed by another wash cycle.
311 The slides were then air dried and mounted with 85% glycerol prior to imaging.
312

313 **Automated imaging**

314
315 Images of stained H&E tissue sections on the ST slides were taken using a Metafer Vslide
316 scanning system (MetaSystems, Germany) installed on an Axio Imager Z2 microscope (Carl Zeiss,
317 Germany) using an LED transmitted light source and a CCD camera (BF scanning). All images
318 were taken with the A-P 10x/0.25 Ph1 objective lens (Carl Zeiss, Germany). For fluorescent
319 scanning, a PhotoFLuor LM-75 lightsource (89North, USA) was used in combination with a Plan-
320 APOCHROMAT 20x/0.8 objective (Carl Zeiss, Germany). A configuration program was made to
321 enable automatic tissue detection, focusing and scanning on all ST arrays present on a glass slide.
322 In short, tissue detection was based on contrast as compared to normalized background in RGB
323 channels. Upon finding maximum contrast in a 12-step spiral-like search window field of view
324 (FOV) pattern, the automated focal alignment in every second of each FOV (4096x3000 px) was
325 initiated. The alignment search considered the maximum contrast z-position as in-focus using 5µm
326 stage intervals (n=19 focal planes). The BF scanning of the predefined ST array areas was done in
327 a total of 48 FOVs and ~30sec in 3 channels (RGB); or fluorescent scanning of 228 FOVs and
328 ~6min for 3 fluorescent channels. Images were stitched using 60µm overlap and linear blending
329 between FOVs with the VSlide software (v1.0.0) and then extracted using jpg compression.
330 Multiple ST slides can be processed in the same manner without any user input for a total of 6min
331 processing time per H&E stained slide (3 channels) or 45min for fluorescently stained slide (3
332 channels), including image stitching.
333

334 **SM-Omics automation**

335

336 The SM-Omics protocol is divided into three main parts. The first part (1) processes all *in*
337 *situ* reactions on a ST slide: tissue pre-permeabilization, permeabilization, reverse transcription
338 with or without the release of the spatial capture probes and tissue removal. This material is
339 collected to a standard 96-well PCR microplate (Eppendorf, Germany) and all of the following
340 reactions (protocols 2 and 3) are run in 96-well plates. The second protocol (2) contains second
341 strand synthesis reaction, cDNA bead purifications and T7 *in vitro* transcription. The third protocol
342 (3) includes aRNA adapter ligation, bead purifications and second cDNA synthesis. The material
343 is then quantified using a standard qPCR protocol and the libraries accordingly indexed for
344 Illumina sequencing.
345

346 Reference material preparation

347
348 In order to test reproducibility of library preparation reactions, we prepared reference
349 material as input. 7.5µg of universal mouse reference RNA (#740100, Agilent Technologies, USA)
350 was fragmented using NEBNext Magnesium RNA fragmentation module (NEB, USA) for 1
351 minute at 94°C. The sample was purified with a MinElute Cleanup kit (Qiagen, Germany)
352 according to manufacturer's instructions and RNA concentration and size were assessed using a
353 Qubit RNA HS kit (ThermoFisher Scientific, USA) and Bioanalyzer Pico 6000 kit (Agilent
354 Technologies, USA), respectively. ~2µg of fragmented RNA was incubated with either 3.3µM
355 custom hexamer primer
356 (GACTCGTAATACGACTCACTATAGGGACACGACGCTCTTCCGATCTNNNNNNNN,
357 T7handle_IlluminaAhandle_hexamer) or poly(d)T primer
358 (T7handle_IlluminaAhandle_hexamer_20TVN) in the presence of 0.8mM dNTP (ThermoFisher
359 Scientific, USA) at 65°C for 5 minutes. First strand reverse transcription was performed with a
360 final concentration of 1X First Strand Buffer, 5 mM DTT, 2U/µl RNaseOUT and 20U/µl of
361 Superscript III (all from Thermo Fisher Scientific, USA). The reaction was incubated at 25°C for
362 10 min (when using hexamer priming), followed by 50°C for 1 hr and 70°C for 15 minutes or 50°C
363 for 1 hr and 70°C for 15 minutes for poly(d)T priming. The reaction was purified with AMPure
364 XP beads (Beckman Coulter, USA) at a beads/DNA ratio of 0.8:1. The concentration of the
365 material was measured on a Qubit RNA HS kit (ThermoFisher Scientific, USA) and diluted in EB
366 (Qiagen, Germany). A release mixture of ~100ng (hexamer priming) or ~200ng (poly(d)T
367 priming) first strand cDNA, 1X Second strand buffer (ThermoFisher Scientific, USA), 0.2µg/µl
368 BSA and 0.5mM dNTP (ThermoFisher Scientific, USA) was used to test all library preparation
369 reactions. Hexamer primed cDNA was used to test the reproducibility and poly(d)T primed cDNA
370 was used to test adapter concentrations and ligation time.
371

372 *in situ* SM-Omics protocol (1)

373
374 Tissue-stained ST slides we provided as input. The ST slide was attached into the ProPlate
375 Multi-Array slide system (GraceBioLabs, USA), with up to four ST slides fitted. The ProPlate
376 Multi-Array system was then fixed in position by Aluminum Heat Transfer Plate (VP 741I6-GS-
377 4, V&P Scientific, Inc, USA) on the Agilent Bravo deck. The protocol started with tissue pre-
378 permeabilization (30 min at 33°C for mouse brain) with addition of 120µl reagent per well of
379 exonuclease I buffer (NEB, USA). In case spleen sections were processed, the pre-
380 permeabilization step was skipped. For complete removal of the reagents and wash solutions from

381 the subarrays all of the robotic dispensing and aspiration steps took place in all four corners of the
382 square wells. Pre-permeabilization reagent removal was followed by a 180µl wash in 0.1X Saline
383 Sodium Citrate (SSC, Sigma-Aldrich, USA) at 33°C. Next, tissue permeabilization was done using
384 75µl 0.1% pepsin (pH 1, Sigma-Aldrich, USA) at 33°C for 10min (mouse brain) and 60min 75µl
385 0.1% pepsin (spleen) prepared at pH 2.5 in Tris-HCl (Sigma-Aldrich, USA). After a 180µl 0.1X
386 SSC wash at 33°C, *in situ* cDNA synthesis reaction was performed by the addition of 75µl RT
387 reagents: 50ng/µl actinomycin D (Sigma-Aldrich, USA), 0.5mM dNTPs (Thermo Fisher
388 Scientific, USA), 0.20µg/µl BSA, 1 U/µl USER enzyme (both from NEB, USA), 6% v/v
389 lymphoprep (STEMCELL Technologies, Canada), 1M betaine (#B0300-1VL, Sigma-Aldrich,
390 USA), 1X First strand buffer, 5mM DTT, 2U/µl RNaseOUT, 20U/µl Superscript III (all from
391 Thermo Fisher Scientific, USA). The reactions were sealed with 70µl of white mineral oil
392 Drakerol#7 (Penreco, USA). Incubation at 30°C was performed for a minimum of 6h, after which
393 70µl of the released material was collected in a new 96-well PCR plate (Eppendorf, Germany).
394 When a Cy3 fluorescent cDNA activity print was needed for tissue optimization, the 75µl *in situ*
395 cDNA reaction mix was as follows: 50ng/µl actinomycin D (Sigma-Aldrich, USA), 0.20µg/µl
396 BSA (NEB, USA), 1X M-MuLV buffer, 5mM DTT, 2U/µl RNaseOUT, 20U/µl M-MuLV (all
397 from Thermo Fisher Scientific, USA), 4µl dNTP mix (dATP; dGTP and dTTP at 10mM and dCTP
398 at 2.5mM) and 2.2µl Cy3-dCTPs (0.2mM, Perkin Elmer, USA).

399

400 ***in situ* manual ST protocol**

401

402 The manual ST *in situ* protocol was performed as described in Salmén *et al*[45]. The
403 protocol is, if not mentioned below, identical to the robotic protocol except as further described.
404 Tissue-stained ST slide was attached in an ArrayIT hybridization chamber (ArrayIT, CA). All
405 incubations took place on an Eppendorf Thermocycler R (Eppendorf, Germany), and reactions
406 were covered with Microseal 'B' PCR Plate Seals (Biorad, CA) to avoid evaporation. Pre-
407 permeabilization and washes were performed with 100µl reagent at 37°C and the *in situ* cDNA
408 synthesis reaction was run without the USER enzyme, lymphoprep and betaine, at 42°C. The
409 manual protocol then encompassed tissue removal and probe release as described[45]. Tissue
410 removal took place in two separate steps with RLT buffer with β-mercaptoethanol and Proteinase
411 K. 80µl of 1% β-mercaptoethanol (Sigma-Aldrich, USA) in RLT buffer (Qiagen, Germany) were
412 added to the wells and incubated at 56°C for 1h. Following removal of the reaction mix and wash
413 with 0.1X SSC solution, 80µl of second tissue removal mixture; 2.5µg/µl Proteinase K in PDK
414 buffer (Qiagen, Germany) were added and the reaction was performed at 56°C for 1h. The
415 complete reaction mix was again removed and a slide wash with one 10 minute wash of the wells
416 with 2X SSC/0.1% SDS (Sigma-Aldrich, USA), followed by 1 minute wash with 0.2X SSC and
417 finally 0.1X SSC was performed. Cleavage of probes from the surface was performed in the next
418 steps and not during *in situ* cDNA synthesis. The reaction mix consisted of 1.1X Second strand
419 buffer (ThermoFisher Scientific, USA), 0.1mM dNTPs and 1 U/µl USER enzyme (NEB, USA).
420 75µl of the mix was added and incubated for 3h at 37°C. The released material was collected in a
421 new 96-well PCR plate (Eppendorf, Germany) by aspirating 70µl of the released material.

422

423 **SM-Omics library preparation (2)**

424

425 Upon initiating the Agilent Bravo form the user was prompted to select either: 1, 2, 3, 4, 6
426 or 12 columns of the 96-well plate to run. Two positions on the Bravo deck had Peltier thermal
427 stations (4-95°C) in the standard 96-well format. A reagent plate was prepared for robotic
428 aspiration, transfer and dispensing of reagents. First, single-stranded cDNA was made to double-
429 stranded material using 5 µl of the reaction mix (2.7X First strand buffer, 3.7 U/µl DNA
430 polymerase I and 0.2 U/µl Ribonuclease H (all from ThermoFisher Scientific, USA)) for 2h at
431 16°C. Thereafter, the material was blunted by the addition of 5µl of 3U/µl T4 DNA polymerase
432 (NEB, USA) for 20 minutes at 16°C. The reaction was stopped by addition of Invitrogen UltraPure
433 0.5M EDTA (pH 8.0, ThermoFisher Scientific, USA) to a final concentration of 20mM. The
434 material was then purified using Ampure XP (Beckman Coulter, USA) at a bead to cDNA ratio of
435 1:1. Next, 27.8µl of the T7 reaction mix (46.2mM rNTPs, 1.5X T7 reaction buffer, 1.54 U/µl
436 SUPERaseIN inhibitor and 2.3U/µl T7 enzyme; all from ThermoFisher Scientific, USA) was
437 added and sealed with 40µl of Vapor-Lock oil (Qiagen, Germany) for an overnight 14h incubation
438 at 37°C. After incubation, 2.1µl of nuclease-free water (ThermoFisher Scientific) was added and
439 the Vapor-Lock was removed, followed by a bead cleanup with RNAClean Ampure XP beads
440 (Beckman Coulter, USA) at a ratio of 1.8:1 of beads:aRNA. The material was then assessed with
441 a Bioanalyzer RNA 6000 Pico kit (Agilent Technologies, USA). 8µl of the eluted 12µl aRNA was
442 transferred into a new 96-well PCR plate (Eppendorf, Germany).

443

444 **SM-Omics library preparation (3)**

445

446 2.5µl of either 3µM (standard) or 15µM aRNA adapters (efficient)
447 [rApp]AGATCGGAAGAGCACACGTCTGAACTCCAGTCAC[ddC] were added to 8µl of
448 aRNA. The reaction was then incubated at 70°C in a PCR machine for 2min and immediately
449 chilled on wet ice. The user then again selected the number of columns they wished to run. 4.5µl
450 T4 RNA ligation mix (3.3X T4 RNA ligase buffer, 66U/µl truncated T4 ligase 2 and 13U/µl
451 murine RNase inhibitor (all from NEB, USA)) were added to the aRNA/adaptor solution. The
452 ligation reaction took place at 25°C for 1h (standard) or 3h (efficient). For the SM-Omics protocol,
453 the ligation reaction was performed for 3h in the presence of 15µM aRNA adapters. The ligation
454 was followed by an Ampure XP (Beckam Coulter, USA) bead purification at a ratio of 1.8:1
455 bead:cDNA. Elution volume was 12µl. After bead purification, 2µl of a primer and dNTP mix (1:1
456 v/v of either 20µM or 40µM GTGACTGGAGTTCAGACGTGTGCTCTTCCGA and 10mM
457 dNTPs) were added to the ligated samples. For the SM-Omics protocol, 40µM primer amount was
458 added using the same volumes. Then, the samples were sealed with 40µl Vapor-Lock (Qiagen,
459 Germany) and heated to 65°C for 5min. The Vapor-Lock was thereafter removed and 8µl of
460 reverse transcription mix were added (2.5X First strand buffer, 13mM DTT, 5 U/µl RNaseOUT
461 and 25 U/µl Superscript III; all from Thermo Fisher Scientific, USA), with the addition of 40µl
462 Vapor-Lock to reseal the reaction. The samples were incubated at 50°C for 1h. 10µl of nuclease-
463 free water was added followed by a final Ampure XP bead purification at 1.7:1 bead:cDNA ratio
464 with a final elution of 10µl nuclease-free water.

465

466 **Staining tissues with oligonucleotide-conjugated antibodies**

467

468 As described above, the fresh frozen tissue was placed on the spatial array slide and fixed
469 at RT, followed by antibody incubations at 4°C. First, tissues were blocked and permeabilized as

470 described above. This was followed by a series of 3 washes in 1X PBS and a last wash that was
471 incubated for 2min. After discarding the wash, oligonucleotide-conjugated antibodies and
472 fluorescently labeled antibodies (Biolegend, USA) were both added at a 1:100 dilution in the same
473 buffer as in the initial permeabilization step and incubated for 1h. The tissue was then washed and
474 the antibody conjugates fixed to the array surface in 4% PFA (Sigma-Aldrich, USA). Tissues were
475 then fluorescently imaged and SM-Omics libraries created. The following steps were added in the
476 library preparations to ensure collection of spatially-barcoded antibody tags. First, cDNA synthesis
477 was performed *in situ* under the same conditions as described above. Next, second strand synthesis
478 was also performed as described followed by an Ampure XP bead clean up as according to
479 manufacturer's instructions. During this clean up, material that would otherwise have been
480 discarded after binding to the beads in standard SM-Omics library preparations, was saved and
481 represented a population of spatially barcoded antibody tags. This elute contained short products
482 that required a bead clean up procedure as well, where a 1.4X bead-to-material ratio was used and
483 the final product eluted in 50 μ L EB (Qiagen, Germany). This material was then indexed for
484 Illumina sequencing using Small RNA Illumina indexes in a KAPA indexing reaction as described
485 in *Quantification, indexing and sequencing*.
486

487 **Manual ST library preparation**

488
489 Manual library preparation was performed as described in Salmén *et al*[45] and included
490 the same experimental steps as the robotic library preparation protocol, but performed manually,
491 incubations took place in a PCR System Eppendorf Mastercycler (Eppendorf, Germany) and
492 instead of Vapor-Lock, reactions were sealed using MicroAmp Optical 8-Cap Strips
493 (ThermoFisher Scientific, USA). The manual procedure also included the following deviations
494 from the robotic library preparation: T7 reaction mix of 18.6 μ l was used and 1.4 μ l of nuclease-
495 free water was added after the 14 hours incubation.
496

497 **Manual Visium preparation**

498
499 Cortical tissues from an adult mouse brain were cryosectioned at 10 μ m thickness and
500 placed on Visium capture areas. The protocol was followed as in the Visium Spatial Gene
501 Expression User Guide CG000239 Rev B as provided by 10X Genomics.

502 503 **Quantification, indexing and sequencing**

504
505 qPCR library quantification and indexing were performed as described in Salmén *et al*[45].
506 The indexed SM-Omics cDNA libraries were diluted with 40 μ l of nuclease-free water to allow for
507 a final library bead cleanup with 0.8:1 ratio Ampure XP beads to PCR products, according to the
508 manufacturer's protocol. Final elution was done in 16 μ l EB (Qiagen, Germany). Individual
509 libraries' fragment lengths and concentrations were evaluated on a Bioanalyzer HS (Agilent
510 Technologies, USA) or DNA1000 TapeStation (Agilent Technologies, USA) and DNA HS Qubit
511 assays (ThermoFisher Scientific, USA), respectively. Samples were then diluted to the desired
512 concentration for sequencing (~1.08 pM final for NextSeq sequencing with 10% PhiX) and
513 sequenced 27-30nt in the forward read and 55-58nt in the reverse read. For antibody tags, the final

514 clean-up was performed at 0.9:1 ratio of beads to PCR products and elution again done in 16µl EB
515 (Qiagen, Germany). Samples were diluted to 8pM final concentration before sequencing on an
516 Illumina Miseq (2x25nt).

517

518 **Raw reads processing and mapping**

519

520 ST, SM-Omics, Visium or antibody tag fastq reads were generated with bcl2fastq2. ST
521 Pipeline[52] v.1.3.1 was used to demultiplex the spatial barcodes and collapse duplicate UMI
522 sequences for ST, SM-Omics and Visium. In short, 5nt trimmed R2 was used for mapping to the
523 mouse genome (mm10) using STAR[53]. After that, mapped reads were annotated using HTseq-
524 count[54]. To collapse UMIs, the annotated reads needed to first be connected to a spatial barcode
525 using a TagGD[55] demultiplexer (k-mer 6, mismatches 2). Then, UMIs mapping to the same
526 transcript and spatial barcode were collapsed using naive clustering with one mismatch allowed in
527 the mapping process. The output file is a genes-by-barcode matrix that was used in all further
528 processing steps. To map antibody tags to their respective spatial barcodes, we used the tag
529 quantification pipeline originally developed for CITE-Seq (v.1.3.2) available at
530 <https://github.com/Hoohm/CITE-seq-Count>. The pipeline was run with default parameters
531 (maximum Hamming distance of 1). We additionally provided the spatial barcodes and corrected
532 the spatial mapping (1 mismatch) for a total of 1007 different barcodes.

533

534 **Automated image processing for spatial transcriptomics**

535

536 For efficient processing, HE images were scaled to approximately 500x500 pixels using
537 the `imagemagick` (<https://imagemagick.org/index.php>) `mogrify` command. In order to reconstruct
538 the positions of all ST spots, visible (*i.e.*, not covered by the tissue section) barcode (x,y) spots
539 were registered through “blob detection” and then refined by keeping only those “blobs” (potential
540 grid points) that were likely to be part of a regular grid. A regular grid was then fitted to the
541 remaining potential grid points, starting an iterative process in which the 0.1% potential grid points
542 that least fit the grid were removed in each iteration and a new grid was fitted until the target
543 number of grid points per row (here 35) and column (here 33) were reached. Finally, those grid
544 points that overlapped the tissue sections were identified by building a mask that represented the
545 tissue area and registering all grid points that were present in this mask. In order to accommodate
546 atypical tissue coloring, bubbles, and smears present as imaging artifacts, we introduced a
547 parameter that toggles the color channels used to detect the tissue section. Finally, an intermediate
548 report notifies the user of irregularities in the automatic alignment process and allows for visual
549 inspection. The output .tsv file contained barcode spots (x,y) as centroid pixel coordinates of the
550 detected grid, as well as a TRUE/FALSE value, set as TRUE if the barcode spot was detected as
551 under the tissue section area.

552

553 **SpoTter Integration with ST Pipeline and Quality Control (QC)** 554 **reporting**

555

556 The following steps integrate the output from the automated image alignment steps with
557 the output gene-by-barcode expression file as produced by the ST Pipeline v.1.3.1. The barcode

558 (x,y) spots approximated as under the tissue section were used for subsetting the ST Pipeline gene-
559 by-barcode file. Then, the original H&E images were downscaled and cropped using the following
560 imagemagick commands: convert HE_image.jpg -crop width"x"height+xa+ya; where width and
561 height represented the Euclidean lengths between (x,y) grid detected barcode spots (33,35), (1,35)
562 and (1,35), respectively. xa and ya were described as the centroid pixel coordinates of the grid
563 point (33,35). The cropped H&E image was then rotated as follows: mogrify -flop -flip
564 HE_image.jpg and this image was then used as input to the QC reporting system and for the GUI
565 annotation tool. A final quality control (QC) report was created when running SpoTter.
566

567 **Comparison of SpoTter vs. ST Spot Detector vs. manual alignment**

568
569 To be able to compare the automated image processing developed here to that of manually
570 processed images, we acquired an additional image of the ST array area after the experiment was
571 performed and the tissue had been removed from the array surface. Briefly, complementary and
572 Cy3 labeled oligonucleotides (IDT, USA) were diluted in 2X SSC with 0.05% SDS to a final
573 concentration of 1 μ M. 50 μ l of the diluted solution was added to the array surface and incubated
574 with shaking (50rpm) for 10min at RT. This was followed by washing the slide in 4XSSC with
575 0.1% SDS and 0.2X SSC. The array frame and all ST barcode positions had then efficiently been
576 labeled and acquired on the same imaging system as described. All input images in the following
577 comparisons were the same approximate input sizes and resolution. The ST spot detector tool
578 previously developed[46] uses the H&E and Cy3 images as input. Due to its intrinsic scaling factor
579 and input image size requirements, initial pre-processing of both images was needed, such that
580 images be linearly downscaled to 30% of their original size and both images individually cropped
581 to represent the same FOVs as collected during the imaging step. However, cropping was only
582 needed if the user did not have the possibility to automatically acquire the same FOVs using the
583 same starting (x,y) positions. For manual alignment, we used Adobe Photoshop for initial pre-
584 processing, same as in the previous step. Both the H&E and Cy3 acquired images were downscaled
585 to 30% of their original size, rotated 180 degrees and aligned to the same starting (x,y) pixel
586 coordinates. This was followed by cropping both images along the middle of the first and last row
587 and column. The tissue boundaries were detected using the magic wand function (32px) and the
588 selected subtracted in the Cy3 image. Spots boundaries were again detected using the same magick
589 wand function and the background noise cleaned up using the bucket fill function (250px) in a
590 grayscale image. This grayscale image was further used in Fiji[56] to detect the centroid
591 coordinates of each ST barcode spot. Following Fiji processing, we translated (x,y) pixel centroid
592 coordinates to ST barcode spot coordinates (as given during the demultiplexing step in the ST
593 pipeline). For SpoTter input, we only provided the original H&E imaged as acquired by the
594 imaging system with no GUI-based preprocessing. For speed comparisons, total time needed for
595 preprocessing steps was measured first. For manual processing, the pre-processing steps included
596 alignment of the H&E and Cy3 images with Adobe Photoshop 2019 and creation of an ST array
597 spots files. For ST Detector pre-processing time, we only took into consideration the time needed
598 to open the same images in Adobe Photoshop, downscale them to 30% size and crop them the
599 same size without any other image handling processes performed. For SpoTter, preprocessing
600 included the downscaling step performed with imagemagick and incorporated into the workflow.
601 Processing steps were then performed and time was measured as described before. Total speed
602 was considered as $1/t$ [s⁻¹] where t represents the sum of time needed for both the pre-processing

603 and processing steps. False positive and negative rates were calculated as percentage of spots
604 present or absent in SpoTteR or ST Detector as compared to manually processed spot coordinates.
605

606 **Estimating lateral diffusion**

607
608 Two consecutive mouse cortex fresh frozen sections were processed. One was processed
609 manually as described earlier[45] while the other was processed using our devised robotic liquid
610 handling setup. For these tests, we created poly(d)T arrays in-house according to manufacturer's
611 instructions (Codelink, Surmodics, USA) using amine-activate slides. The surface area covered
612 with poly(d)T probes was 6x6mm. Both the H&E and gene activity Cy3 images were processed
613 in Fiji[56]. Cell boundaries were detected (Analyze > Plot Profile) with 10% signal intensity and
614 these were used as breakpoints to estimate Cy3 signal diffusion as lateral diffusion. Left and right
615 cell boundaries (detected as local maxima in respective images) representing opposite sides of
616 each cell were used in the estimate and a total of 50 cells used in each condition. A 0.1728 pixel
617 to distance conversion ratio was used. If a diffusion distance measure was scored as negative it
618 implied that the Cy3 signal was contained within the detected cell boundaries, and positive if
619 outside those same boundaries.
620

621 **Estimating reproducibility of SM-Omics *in situ* reactions**

622
623 Scikit-image[57] was used to process the H&E and respective fluorescent gene expression
624 images. First, a grayscale fluorescent image was smoothed using a Gaussian filter (sigma=0.01).
625 Then, we applied morphological reconstruction by dilating the image edges through filtering its
626 regional maxima. This enabled us to create a background image value that could be subtracted
627 from the original image and used in further analysis. Then, we created an elevation map with a
628 sobel filter to mask the elevated points. This image could then be used in a tissue (*i.e.*, object)
629 detection step using watershedding. The inverted tissue boundaries were subtracted from the
630 detected fluorescent tissue gene expression signals and used in all further analysis. The medians
631 of the fluorescent signals were compared using a Wilcoxon ranked sum test.
632

633 **Image annotation**

634
635 To manually annotate tissue images based on their H&E features, we used a previously
636 adapted graphical and cloud-based user interface[26]. We assigned each ST (x,y) coordinate with
637 one or more regional tags. The region names used to annotate MOB were: Granular Cell Layer
638 (GR), Outer Plexiform Layer (OPL), Mitral Layer (MI), Internal Plexiform Layer (IPL) and
639 Glomerular Layer (GL) and to annotate mouse cortex were: Cerebral nuclei (CNU), Cortical
640 subplate (CTXsp), Fiber tracts, Hippocampal formation (HIP), Hypothalamus (HY), Isocortex
641 (ISOCTX), Midbrain (MB), Piriform area (PIR) and Thalamus (TH). For annotating spleen, we
642 used four major areas: Red pulp, B-follicle, Marginal zone and Periarteriolar lymphoid sheaths
643 (PALS).
644

645 **Comparisons between spatial gene expression profiles**

646

647 For comparisons between the SM-Omics and ST datasets, reads were first downsampled to
648 the same saturation level (64%; chosen based on estimated saturation curve) before invoking a ST
649 pipeline mapper, annotator and counter run to receive UMIs per spatial (x,y) barcode as described
650 previously. Depending on sequencing depth, a gene was counted as expressed if the corresponding
651 transcript was present in more than 10^{-6} of the sequencing depth. The total count over all spots per
652 gene and sample were then normalized[58]. Pearson's correlation coefficient between the average
653 and normalized samples as well as the Wilcoxon's rank-sum tests was calculated using Scipy
654 v1.2.0[59]. To compare the performance of Visium and SM-Omics, we sequenced both libraries
655 to an average depth of ~65 million paired end reads. For Visium, we sequenced 29 nt in the forward
656 and 43 nt in the reverse read. Reads were downsampled to the same saturation level. Both datasets
657 were processed using the ST pipeline as described above. Briefly, we mapped reads to the modified
658 transcriptome reference as suggested and following instructions by 10X Genomics. Conventional
659 GTF files used in the annotation step with HTseq-count were converted so that all transcript
660 features now carried an exon tag used in counting transcripts. UMI collapsing was done using a
661 naive approach and allowing for 1 low quality base present in either of the datasets. Unique
662 molecular identifiers (UMI) per measurement were calculated as previously described[52].
663

664 **Saturation curve generation**

665
666 Number of unique molecules was calculated by subsampling the same proportion of
667 mapped and annotated reads from each sample and then ran the samples through ST Pipeline
668 v.1.3.1, where unique molecules were calculated as previously described.
669

670 **Calculating quantitative immunofluorescence profiles per SM-Omics** 671 **spot**

672
673 First, we trained a random forest classifier using the Ilastik[60] framework to extract
674 probabilities of the positive class assignment ie. positive antibody signals from our IF mouse brain
675 images. Separate classifiers were trained to each antibody used and a total of ~10 images with at
676 least 10 fields of view were used in the training process. In each classifier, we used two labels for
677 classification: signal and background. Respective full-sized fluorescent microscopy images were
678 then processed and output probabilities used in the following steps. For spleen data, raw
679 fluorescent images were used as input in the following steps. First, images were processed as
680 described in *Estimating reproducibility of SM-Omics in situ reactions*. Calculated background was
681 removed from each image, signal boundaries estimated using watershedding followed by creating
682 a binary mask image. This mask was then overlaid with the original fluorescent image and this
683 image was then used in all following steps. To quantify the fluorescent signal intensities per ST
684 spot, the image was cropped into a 33x35 matrix creating smaller patches; each patch sized at $\pm 1\%$
685 image from the centroid of each ST spot. Finally, the intensity from each spot area was calculated
686 as the sum of the fluorescent signal detected in that spot patch.
687

688 **Spatial gene and antibody-based expression analysis**

689

690 Statistical analysis of the spatial gene and antibody tag expression data was performed
691 using Splotch' one- or two-level hierarchical model as previously described[31]. In short, the
692 model captures spatial expression in anatomical regions while accounting for experimental
693 parameters such as, in our case, different animals, and calculates gene or antibody expression
694 estimates for each single gene or antibody in each annotated spatial spot. To find targets which
695 were differentially expressed in an annotated morphological region, we computed a one-vs-all
696 comparison and took those values with a positive log Bayesian factor (BF). Expression estimates
697 from Splotch were used when calculating the correlation between gene expression and antibody
698 tag counts. The expression and counts mean were calculated per annotated region and then scaled
699 from 0 to 1 within each sample. The correlation between gene expression and fluorescent signal
700 was calculated in the same way, but the fluorescent signal matrix, prepared as explained in
701 *Calculating quantitative immunofluorescence profiles per SM-Omics spot*, was used instead of the
702 antibody tag counts matrix.
703

704 **Comparison to Allen Brain Atlas data**

705
706 To validate our findings, we downloaded ISH gene expression data from four major
707 regions; GL, GR, MI and OPL, from the Allen Brain Atlas (ABA) (<https://mouse.brain-map.org/>).
708 For comparison in cortex samples, we used the following regions from ABA: piriform-amygdalar
709 area (PAA), postpiriform transition area (TR) in addition to CNU, STXsp, HIP, HY, ISOCTX,
710 MB and TH. Prior to enrichment analysis, genes found in PAA, TR and PIR in ABA were merged
711 into one region name: PIR. We filtered genes with fold change >1 and expression threshold >2.5
712 in ABA and compared to genes with positive fold change and log(BF) in our Splotch data and
713 computed a one-sided Fisher's exact test using Scipy v1.2.0[59]. FDR was estimated using the
714 Benjamini-Hochberg[61] procedure. One of the top most differentially expressed genes in both
715 SM-Omics and ABA was chosen from each region and its expression visualized. The
716 visualizations were compared to the corresponding *in situ* hybridization (ISH) images, downloaded
717 from the ABA webpage. A reference ST dataset[24] was also analyzed using Splotch with the
718 same settings as used for SM-Omics, visualized and compared to SM-Omics.
719

720 **Data and code availability**

721 Raw and processed data will be available at the Single Cell Portal
722 (https://portals.broadinstitute.org/single_cell/study/SCP979).
723

724 **Acknowledgments**

725
726 We thank Ania Hupalowska for making all graphical illustrations. We thank Tarmö Äijö
727 for help with Splotch and Theresa Teneyck for help with Bravo protocol implementation. Work
728 was supported by the Knut and Alice Wallenberg Foundation, the Royal Swedish Academy of
729 Sciences and Swedish Society for Medical Research (S.V.), the Hans Werthén Foundation (B.L),
730 HFSP long term fellowship (LT000452/2019-L) (J.K.), the Klarman Cell Observatory, the Manton
731 Foundation, and HHMI (A.R.). S.V is supported as a Wallenberg Fellow at the Broad Institute of
732 MIT and Harvard.
733

734 **Author contributions**

735
736 S.V. and A.R. designed the study and experiments; S.V. and B.L. performed the
737 experiments with help from Å.S. for the automation testing steps; S.V. and J.K. designed and
738 implemented the automatic alignment and reporting tool; B.L. analyzed data with supervision from
739 S.V.; O.R.R. helped plan experiments. S.V., B.L. and A.R. wrote the manuscript with input from
740 all the authors. All authors discussed the results.

742 **Competing interests**

743
744 A.R. is a founder and equity holder of Celsius Therapeutics, an equity holder in Immunitas
745 Therapeutics and until August 31, 2020 was an SAB member of Syros Pharmaceuticals, Neogene
746 Therapeutics, Asimov and ThermoFisher Scientific. From August 1, 2020, A.R. is an employee of
747 Genentech. S.V. and A.R. are co-inventors on PCT/US2020/015481 relating to this work.

749 **References**

- 750
- 751 1. Jovanovic M, Rooney MS, Mertins P, Przybylski D, Chevrier N, Satija R, et al.
752 Immunogenetics. Dynamic profiling of the protein life cycle in response to pathogens.
753 *Science*. 2015;347: 1259038.
 - 754 2. Rabani M, Raychowdhury R, Jovanovic M, Rooney M, Stumpo DJ, Pauli A, et al. High-
755 resolution sequencing and modeling identifies distinct dynamic RNA regulatory strategies.
756 *Cell*. 2014;159: 1698–1710.
 - 757 3. Chick JM, Munger SC, Simecek P, Huttlin EL, Choi K, Gatti DM, et al. Defining the
758 consequences of genetic variation on a proteome-wide scale. *Nature*. 2016. pp. 500–505.
759 doi:10.1038/nature18270
 - 760 4. Zhang B, Wang J, Wang X, Zhu J, Liu Q, Shi Z, et al. Proteogenomic characterization of
761 human colon and rectal cancer. *Nature*. 2014;513: 382–387.
 - 762 5. Stoeckius M, Hafemeister C, Stephenson W, Houck-Loomis B, Chattopadhyay PK,
763 Swerdlow H, et al. Simultaneous epitope and transcriptome measurement in single cells.
764 *Nat Methods*. 2017;14: 865–868.
 - 765 6. Zheng GXY, Terry JM, Belgrader P, Ryvkin P, Bent ZW, Wilson R, et al. Massively
766 parallel digital transcriptional profiling of single cells. *Nat Commun*. 2017;8: 14049.
 - 767 7. Macosko EZ, Basu A, Satija R, Nemes J, Shekhar K, Goldman M, et al. Highly Parallel
768 Genome-wide Expression Profiling of Individual Cells Using Nanoliter Droplets. *Cell*.
769 2015;161: 1202–1214.
 - 770 8. Klein AM, Mazutis L, Akartuna I, Tallapragada N, Veres A, Li V, et al. Droplet barcoding

- 771 for single-cell transcriptomics applied to embryonic stem cells. *Cell*. 2015;161: 1187–1201.
- 772 9. Habib N, Li Y, Heidenreich M, Swiech L, Avraham-Davidi I, Trombetta JJ, et al. Div-Seq:
773 Single-nucleus RNA-Seq reveals dynamics of rare adult newborn neurons. *Science*.
774 2016;353: 925–928.
- 775 10. Habib N, Avraham-Davidi I, Basu A, Burks T, Shekhar K, Hofree M, et al. Massively
776 parallel single-nucleus RNA-seq with DroNc-seq. *Nat Methods*. 2017;14: 955–958.
- 777 11. Slyper M, Porter CBM, Ashenberg O, Waldman J, Drokhyansky E, Wakiro I, et al. A
778 single-cell and single-nucleus RNA-Seq toolbox for fresh and frozen human tumors. *Nat*
779 *Med*. 2020;26: 792–802.
- 780 12. Darmanis S, Gallant CJ, Marinescu VD, Niklasson M, Segerman A, Flamourakis G, et al.
781 Simultaneous Multiplexed Measurement of RNA and Proteins in Single Cells. *Cell Reports*.
782 2016. pp. 380–389. doi:10.1016/j.celrep.2015.12.021
- 783 13. Hanahan D, Coussens LM. Accessories to the crime: functions of cells recruited to the
784 tumor microenvironment. *Cancer Cell*. 2012;21: 309–322.
- 785 14. Bodenmiller B. Multiplexed Epitope-Based Tissue Imaging for Discovery and Healthcare
786 Applications. *Cell Syst*. 2016;2: 225–238.
- 787 15. Chen KH, Boettiger AN, Moffitt JR, Wang S, Zhuang X. RNA imaging. Spatially resolved,
788 highly multiplexed RNA profiling in single cells. *Science*. 2015;348: aaa6090.
- 789 16. Lubeck E, Coskun AF, Zhiyentayev T, Ahmad M, Cai L. Single-cell in situ RNA profiling
790 by sequential hybridization. *Nature methods*. 2014. pp. 360–361.
- 791 17. Eng C-HL, Lawson M, Zhu Q, Dries R, Koulena N, Takei Y, et al. Transcriptome-scale
792 super-resolved imaging in tissues by RNA seqFISH. *Nature*. 2019;568: 235–239.
- 793 18. Lee JH, Daugharthy ER, Scheiman J, Kalhor R, Yang JL, Ferrante TC, et al. Highly
794 multiplexed subcellular RNA sequencing in situ. *Science*. 2014;343: 1360–1363.
- 795 19. Goltsev Y, Samusik N, Kennedy-Darling J, Bhate S, Hale M, Vazquez G, et al. Deep
796 Profiling of Mouse Splenic Architecture with CODEX Multiplexed Imaging. *Cell*.
797 2018;174: 968–981.e15.
- 798 20. Keren L, Bosse M, Marquez D, Angoshtari R, Jain S, Varma S, et al. A Structured Tumor-
799 Immune Microenvironment in Triple Negative Breast Cancer Revealed by Multiplexed Ion
800 Beam Imaging. *Cell*. 2018;174: 1373–1387.e19.
- 801 21. Codeluppi S, Borm LE, Zeisel A, La Manno G, van Lunteren JA, Svensson CI, et al. Spatial
802 organization of the somatosensory cortex revealed by osmFISH. *Nat Methods*. 2018;15:
803 932–935.
- 804 22. Moffitt JR, Bambah-Mukku D, Eichhorn SW, Vaughn E, Shekhar K, Perez JD, et al.

- 805 Molecular, spatial, and functional single-cell profiling of the hypothalamic preoptic region.
806 Science. 2018;362. doi:10.1126/science.aau5324
- 807 23. Ke R, Mignardi M, Pacureanu A, Svedlund J, Botling J, Wählby C, et al. In situ sequencing
808 for RNA analysis in preserved tissue and cells. Nat Methods. 2013;10: 857–860.
- 809 24. Ståhl PL, Salmén F, Vickovic S, Lundmark A, Navarro JF, Magnusson J, et al.
810 Visualization and analysis of gene expression in tissue sections by spatial transcriptomics.
811 Science. 2016;353: 78–82.
- 812 25. Rodriques SG, Stickels RR, Goeva A, Martin CA, Murray E, Vanderburg CR, et al. Slide-
813 seq: A scalable technology for measuring genome-wide expression at high spatial
814 resolution. Science. 2019;363: 1463–1467.
- 815 26. Vickovic S, Eraslan G, Salmén F, Klughammer J, Stenbeck L, Schapiro D, et al. High-
816 definition spatial transcriptomics for in situ tissue profiling. Nat Methods. 2019;16: 987–
817 990.
- 818 27. Wang X, Allen WE, Wright MA, Sylwestrak EL, Samusik N, Vesuna S, et al. Three-
819 dimensional intact-tissue sequencing of single-cell transcriptional states. Science. 2018;361.
820 doi:10.1126/science.aat5691
- 821 28. Thrane K, Eriksson H, Maaskola J, Hansson J, Lundeberg J. Spatially Resolved
822 Transcriptomics Enables Dissection of Genetic Heterogeneity in Stage III Cutaneous
823 Malignant Melanoma. Cancer Res. 2018;78: 5970–5979.
- 824 29. Asp M, Salmén F, Ståhl PL, Vickovic S, Felldin U, Löfling M, et al. Spatial detection of
825 fetal marker genes expressed at low level in adult human heart tissue. Sci Rep. 2017;7:
826 12941.
- 827 30. Asp M, Giacomello S, Larsson L, Wu C, Fürth D, Qian X, et al. A Spatiotemporal Organ-
828 Wide Gene Expression and Cell Atlas of the Developing Human Heart. Cell. 2019;179:
829 1647–1660.e19.
- 830 31. Maniatis S, Äijö T, Vickovic S, Braine C, Kang K, Mollbrink A, et al. Spatiotemporal
831 dynamics of molecular pathology in amyotrophic lateral sclerosis. Science. 2019;364: 89–
832 93.
- 833 32. Berglund E, Maaskola J, Schultz N, Friedrich S, Marklund M, Bergensträhle J, et al. Spatial
834 maps of prostate cancer transcriptomes reveal an unexplored landscape of heterogeneity.
835 Nat Commun. 2018;9: 2419.
- 836 33. Berglund E, Saarenpää S, Jemt A, Gruselius J, Larsson L, Bergensträhle L, et al.
837 Automation of Spatial Transcriptomics library preparation to enable rapid and robust
838 insights into spatial organization of tissues. BMC Genomics. 2020;21: 298.
- 839 34. Jemt A, Salmén F, Lundmark A, Mollbrink A, Fernández Navarro J, Ståhl PL, et al. An
840 automated approach to prepare tissue-derived spatially barcoded RNA-sequencing libraries.

- 841 Sci Rep. 2016;6: 37137.
- 842 35. Vickovic S, Ståhl PL, Salmén F, Giatrellis S, Westholm JO, Mollbrink A, et al. Massive and
843 parallel expression profiling using microarrayed single-cell sequencing. *Nat Commun.*
844 2016;7: 13182.
- 845 36. Lein E, Borm LE, Linnarsson S. The promise of spatial transcriptomics for neuroscience in
846 the era of molecular cell typing. *Science.* 2017;358: 64–69.
- 847 37. Gerdes MJ, Sevinsky CJ, Sood A, Adak S, Bello MO, Bordwell A, et al. Highly
848 multiplexed single-cell analysis of formalin-fixed, paraffin-embedded cancer tissue. *Proc*
849 *Natl Acad Sci U S A.* 2013;110: 11982–11987.
- 850 38. Lin J-R, Fallahi-Sichani M, Sorger PK. Highly multiplexed imaging of single cells using a
851 high-throughput cyclic immunofluorescence method. *Nat Commun.* 2015;6: 8390.
- 852 39. Angelo M, Bendall SC, Finck R, Hale MB, Hitzman C, Borowsky AD, et al. Multiplexed
853 ion beam imaging of human breast tumors. *Nat Med.* 2014;20: 436–442.
- 854 40. Giesen C, Wang HAO, Schapiro D, Zivanovic N, Jacobs A, Hattendorf B, et al. Highly
855 multiplexed imaging of tumor tissues with subcellular resolution by mass cytometry. *Nat*
856 *Methods.* 2014;11: 417–422.
- 857 41. Merritt CR, Ong GT, Church SE, Barker K, Danaher P, Geiss G, et al. Multiplex digital
858 spatial profiling of proteins and RNA in fixed tissue. *Nat Biotechnol.* 2020;38: 586–599.
- 859 42. Schulz D, Zanotelli VRT, Fischer JR, Schapiro D, Engler S, Lun X-K, et al. Simultaneous
860 Multiplexed Imaging of mRNA and Proteins with Subcellular Resolution in Breast Cancer
861 Tissue Samples by Mass Cytometry. *Cell Syst.* 2018;6: 531.
- 862 43. Fisher S, Barry A, Abreu J, Minie B, Nolan J, Delorey TM, et al. A scalable, fully
863 automated process for construction of sequence-ready human exome targeted capture
864 libraries. *Genome Biol.* 2011;12: R1.
- 865 44. Rohland N, Reich D. Cost-effective, high-throughput DNA sequencing libraries for
866 multiplexed target capture. *Genome Res.* 2012;22: 939–946.
- 867 45. Salmén F, Ståhl PL, Mollbrink A, Navarro JF, Vickovic S, Frisén J, et al. Barcoded solid-
868 phase RNA capture for Spatial Transcriptomics profiling in mammalian tissue sections. *Nat*
869 *Protoc.* 2018;13: 2501–2534.
- 870 46. Wong K, Navarro JF, Bergenstråhle L, Ståhl PL, Lundeberg J. ST Spot Detector: a web-
871 based application for automatic spot and tissue detection for spatial Transcriptomics image
872 datasets. *Bioinformatics.* 2018;34: 1966–1968.
- 873 47. Äijö T, Maniatis S, Vickovic S, Kang K, Cuevas M, Braine C, et al. Splotch: Robust
874 estimation of aligned spatial temporal gene expression data. doi:10.1101/757096

- 875 48. Lein ES, Hawrylycz MJ, Ao N, Ayres M, Bensinger A, Bernard A, et al. Genome-wide
876 atlas of gene expression in the adult mouse brain. *Nature*. 2007;445: 168–176.
- 877 49. TotalSeq™. [cited 7 Jul 2020]. Available: <https://www.biolegend.com/en-us/totalseq>
- 878 50. Nagayama S, Homma R, Imamura F. Neuronal organization of olfactory bulb circuits. *Front*
879 *Neural Circuits*. 2014;8: 98.
- 880 51. Zeisel A, Hochgerner H, Lönnerberg P, Johnsson A, Memic F, van der Zwan J, et al.
881 *Molecular Architecture of the Mouse Nervous System*. *Cell*. 2018;174: 999–1014.e22.
- 882 52. Navarro JF, Sjöstrand J, Salmén F, Lundeberg J, Ståhl PL. ST Pipeline: an automated
883 pipeline for spatial mapping of unique transcripts. *Bioinformatics*. 2017;33: 2591–2593.
- 884 53. Dobin A, Davis CA, Schlesinger F, Drenkow J, Zaleski C, Jha S, et al. STAR: ultrafast
885 universal RNA-seq aligner. *Bioinformatics*. 2013;29: 15–21.
- 886 54. Anders S, Pyl PT, Huber W. HTSeq--a Python framework to work with high-throughput
887 sequencing data. *Bioinformatics*. 2015;31: 166–169.
- 888 55. Costea PI, Lundeberg J, Akan P. TagGD: fast and accurate software for DNA Tag
889 generation and demultiplexing. *PLoS One*. 2013;8: e57521.
- 890 56. Schindelin J, Arganda-Carreras I, Frise E, Kaynig V, Longair M, Pietzsch T, et al. Fiji: an
891 open-source platform for biological-image analysis. *Nat Methods*. 2012;9: 676–682.
- 892 57. van der Walt S, Schönberger JL, Nunez-Iglesias J, Boulogne F, Warner JD, Yager N, et al.
893 scikit-image: image processing in Python. *PeerJ*. 2014;2: e453.
- 894 58. Svensson V, Teichmann SA, Stegle O. SpatialDE: identification of spatially variable genes.
895 *Nat Methods*. 2018;15: 343–346.
- 896 59. Jones E, Peterson P, Oliphant T. SciPy: Open Source Scientific Tools for Python. In: *Scipy*
897 [Internet]. 2001. Available: <http://www.scipy.org/>
- 898 60. Berg S, Kutra D, Kroeger T, Straehle CN, Kausler BX, Haubold C, et al. ilastik: interactive
899 machine learning for (bio)image analysis. *Nat Methods*. 2019;16: 1226–1232.
- 900 61. Benjamini Y, Hochberg Y. Controlling the False Discovery Rate: A Practical and Powerful
901 Approach to Multiple Testing. *Journal of the Royal Statistical Society: Series B*
902 (Methodological). 1995. pp. 289–300. doi:10.1111/j.2517-6161.1995.tb02031.x

903 **Figure captions**

904
905 **Fig1. SM-Omics method creates tissue specific spatial gene expression patterns. (a)** SM-Omics
906 approach combines automated imaging of H&E, IF stained or tissue sections stained with DNA-barcoded
907 antibodies with high-throughput liquid handling to create spatially resolved RNA-seq and/or antibody-seq

908 libraries. The RNA-seq protocol consists of three main steps. (I) *in situ* reactions on a ST slide that include
909 tissue permeabilization, capture of mRNAs on the spatial array followed by a reverse transcription reaction
910 in solution. The transcribed material is then collected and a two-step library preparation protocol (II-III) is
911 run in standard 96-well plates. (b) Examples of SM-Omics spatial gene expression patterns (color scale)
912 detected in each of the major histological regions in the main olfactory bulb of an adult mouse brain and
913 (c) corresponding ISH images from ABA for the same genes as in (b) with illustrated and highlighted region
914 annotation patterns. Annotated region abbreviations: GL (Glomerular Layer), GR (Granular Cell Layer),
915 MI (Mitral Layer), OPL (Outer Plexiform Layer) and ONL (Olfactory Nerve Layer) are shared between the
916 panels.

917
918 **Fig2. SM-Omics method tissue specific gene and IF antibody expression patterns.** (a) Tissue sections
919 are placed on the spatial array (I), stained for nuclear and corresponding antigen targets, imaged for
920 fluorescent IF signals (II) and SM-Omics libraries created (III). Spatial gene and antibody expression data
921 are processed and compared to the reference ABA atlas (IV). (b) Neuronal target NeuN; was stained for
922 antibody IF and DAPI and corresponding gene activity labeled (cDNA) confirming feasibility of *in situ*
923 reaction conditions for IF staining. ABA reference image for the same target with labeled zoomed-in area
924 (isocortex). (c) Fluorescently stained tissue section (upper left) could be analyzed and protein IF signals
925 (color scale) aggregated in SM-Omics-like spots (NeuN IF; lower left) for comparison to mRNA expression
926 signals (NeuN mRNA; lower right). White dashed lines circle lower part of the mouse brain *ie.*
927 hypothalamus. Correlation between scaled NeuN IF and respective NeuN mRNA expression per tissue
928 section (n=3; upper right). Each dot represents the mean scaled signal of all SM-Omics spatial
929 measurements in that annotated region (color code). Line (black) represents the linear regression line
930 between the conditions with respective standard deviations (gray dashed lines). Annotated region
931 abbreviations: CTXSP (Cortical subplate), FIB (Fiber tracts), HY (Hypothalamus), HIP (Hippocampal
932 formation), ISOCTX (Isocortex), PIR (Piriform areas) and TH (Thalamus).

933
934 **Fig3. Highly-multiplexed SM-Omics tissue specific gene and antibody expression patterns.** (a) SM-
935 Omics approach combines automated imaging of IF antibody stained tissue sections, tagging antigens
936 spatially *in situ* using barcoded antibodies and capturing mRNA on a spatially barcoded poly(d)T array.
937 Frozen tissue sections are placed on a SM-Omics array, tissues stained with both IF and DNA-tagged
938 antibodies, imaged and *in situ* copying reactions performed and at the same time as cDNA made (I). Then,
939 both the antibody tags and cDNAs are used in the library preparation reactions and sequenced (II). Finally,
940 spatial IF, antibody tag and gene expression patterns can be evaluated (III). (b) Splenic tissue illustration
941 of red and white pulp structures followed by spatial expression profiles of sequenced antibody tags as well
942 as IF images in splenic tissue for F4/80 staining red pulp macrophages and IgD staining marginal zone B
943 cells in the white pulp. (c) Spatial expression profiles (color scale) for a 6-plex SM-Omics reaction with
944 F4/80, IgD, CD163, CD38, CD4 and CD8a DNA-barcoded antibody-based expression in the top panel and
945 respective gene expression shown in the bottom panel.

946

947 Supporting information

948
949 **FigS1. Feasibility of SM-Omics *in situ* reactions.** (a) SM-Omics approach combines automated imaging
950 of H&E (or IF) stained tissue sections to create spatially resolved cDNA expression footprints. First, brain
951 sections are deposited on a mock array with poly(d)T capture area (I) and stained for H&E histology (II).

952 Then, mRNAs are captured on the mock slide and cDNA molecules *in situ* fluorescently labeled (III) to
953 create a spatial cDNA gene expression footprint (IV). **(b)** and **(b')** H&E images of the cortex region on the
954 adult mouse brain for manually prepared samples; coronal brain half and zoomed in region respectively.
955 **(c)** and **(c')** Fluorescent gene activity cDNA footprints corresponding to **(b)** and **(b')**. **(d)** and **(d')** H&E
956 image of the adjacent cortex region processed with SM-Omics; coronal brain half and zoomed in region
957 respectively. **(e)** and **(e')** Fluorescent gene activity footprints corresponding to **(c)** and **(c')**. **(f-g)** Histograms
958 of distances between detected H&E cell boundaries and fluorescent prints for ST and SM-Omics
959 preparations marking lateral diffusion metrics. Solid red lines represent mean and dashed lines standard
960 deviations of the distributions (n=100).

961

962 **FigS2. Evaluation of automated *in situ* reactions within and between SM-Omics runs on MOB tissues.**

963 **(a)** H&E images followed by detected fluorescent (cDNA) footprints (**Methods**) reflecting gene activity in
964 the tissue sample. Each image combination (H&E and cDNA) denotes a respective position (1-3) used
965 during one SM-Omics *in situ* optimization run (upper panel). Histograms of fluorescent tissue footprints
966 detected in one SM-Omics run using three slide positions (lower panel). No significant differences were
967 detected between the medians of the distributions (Wilcoxon's rank-sum test, $p>0.05$). **(b)** Histograms of
968 replicate fluorescent tissue footprints (cDNA) detected (**Methods**) in one SM-Omics run and slide position.
969 No significant differences were detected between the medians of the distributions (Wilcoxon's rank-sum
970 test, $p>0.05$). **(c)** H&E images followed by detected fluorescent (cDNA) footprints (**Methods**) reflecting
971 gene activity in the tissue sample. Each image combination represents a result from a separate SM-Omics
972 run. Histograms of fluorescent tissue footprints detected between three runs. No significant differences
973 were detected between the medians of the distributions (Wilcoxon rank-sum test, $p>0.05$).

974

975 **FigS3. Performing SM-Omics *in situ* reactions on different tissue types. (a-a')** H&E and fluorescent
976 print for the main olfactory bulb of the adult mouse brain. **(b-b')** H&E and fluorescent print for the MC38-
977 OVA inject adoeed cell lines into a preclinical model of colorectal cancer. **(c-c')** H&E and fluorescent print
978 for the adult mouse colon.

979

980 **FigS4. Tissue and array grid detection with SpoTteR. (a)** The RGB tissue H&E stained image as input.
981 The RGB image is split into 3 color channels and circular features are detected. Those features that fit a
982 grid pattern (33x35 matrix) are used for the initial fit. Then circular features outside the grid are removed
983 and the process of grid fitting repeated until a perfect 33x35 matrix is adjusted and positioned. Then the
984 tissue is detected and grid spots under the tissue are easily subtracted. **(b)** SpoTteR performance for tissue
985 and grid detection in three different tissue types: human lung cancer, mouse colon and mouse brain.

986

987 **FigS5. SpoTteR performance. (a)** H&E image with corresponding false negative and positive ST barcode
988 spot (x,y) positions using SpoTteR (blue cross) or ST Detector (black circle) as compared to the manually
989 curated positions (filled red circle) for a mouse colon sample. **(b)** Total false negative and positive rates per
990 processed tissue type. **(c)** Processing speed (given as $1/\text{time}$ [s^{-1}]) for three tested processing approaches
991 with note that there is no hands-on processing needed with SpoTteR while the other approaches require
992 additional user input in either pre-processing or processing steps (**Methods**).

993

994 **FigS6. SM-Omics metrics comparisons to other array versions. (a)** Total number of expressed genes
995 and their intersection and total number of unique molecules detected under the tissue boundaries for SM-

996 Omics (n=3, blue) and ST (n=3, red). **(b)** Number of expressed genes and unique molecules detected per
997 spot under and outside of the tissue boundaries for SM-Omics (n=3, blue) and ST (n=3, red). **(c)** Correlation
998 of the normalized pseudo-bulk gene expressions between SM-Omics (n=3) and ST (n=3). Denoted is the
999 Pearson's correlation coefficient (r) between replicates. Colored line represents the linear regression line
1000 between the replicates. **(d)** Saturation curves as mean proportion value of unique molecules detected per
1001 annotated morphological region with 68% confidence interval in SM-Omics (blue line, n=3) and ST (red
1002 line, n=3). **(e)** Saturation curves (downsampled raw data, **Methods**) depicting total number of detected
1003 UMIs between SM-Omics (blue line, n=3) and Visium (green line, n=3) with 68% confidence interval.
1004 Total number of detected genes **(f)** and UMIs **(g)** per spot under and outside of the tissue boundaries in SM-
1005 Omics (n=3, blue) and Visium (green, n=3) at highest available sequencing saturation point. Annotated
1006 region abbreviations: GL (Glomerular Layer), GR (Granular Cell Layer), MI (Mitral Layer), IPL (Internal
1007 Plexiform layer) and OPL (Outer Plexiform Layer). Nissl stain and corresponding annotation regions shown
1008 in each subplot **(a-d)**, positive region shown in green and rest in gray) as an example from the Allen Brain
1009 Atlas data. Color legend **(a-d)** is shared between the panels as denoted in **(b)**. Color legend **(e-g)** is shared
1010 between the panels as denoted in **(e)**. **(a-d)** represents data from adult mouse MOB and **(e-g)** from adult
1011 mouse cortex. Statistical significance markings (Wilcoxon's rank sum test) are displayed;
1012 $0.01 < p \leq 0.05$ (*). Center line, median; box limits, upper and lower quartiles; whiskers, 1.5x interquartile
1013 range in **(a-b, f-g)** and density past extreme data points in **(a-b)**.

1014
1015 **FigS7. Performance of automated spatial library preparation reactions.** **(a)** Mean fragment length
1016 distribution with 68% confidence interval of amplified RNA for SM-Omics samples (n=3) from three
1017 separate runs. This step represents QC results after the first part of the library preparation. **(b)** Quantitative
1018 concentrations (Cq) reflecting the final library and second part of the automatic preparation for samples
1019 processed in **(a)** from three separate runs. Results display no significant variance between the runs
1020 ($p \geq 0.05$ (ns), Wilcoxon's rank-sum test). **(c)** Impact of ligation reaction times and adaptor concentrations
1021 on mean fragment length distribution with 68% confidence interval of variations of final spatial libraries
1022 prepared using the automated preparation platform (n=3 for "ST 1h ligation", "ST 3h ligation", "SM-
1023 Omics" and n=2 for "ST 1h ligation + adapters") **(d)** Impact of ligation reaction times and
1024 adaptor concentrations on quantitative concentrations (Cq) values for
1025 automated prepared libraries (n=9). Cq values were measured at Fluorescent
1026 unit 10,000. Statistical significance (Wilcoxon's rank-sum test) markings are
1027 displayed: $0.05 < p \leq 1$ (ns), $0.001 < p \leq 0.01$ (**), $0.0001 < p \leq 0.001$ (***). Individual reaction
1028 conditions have been detailed in **Methods**.

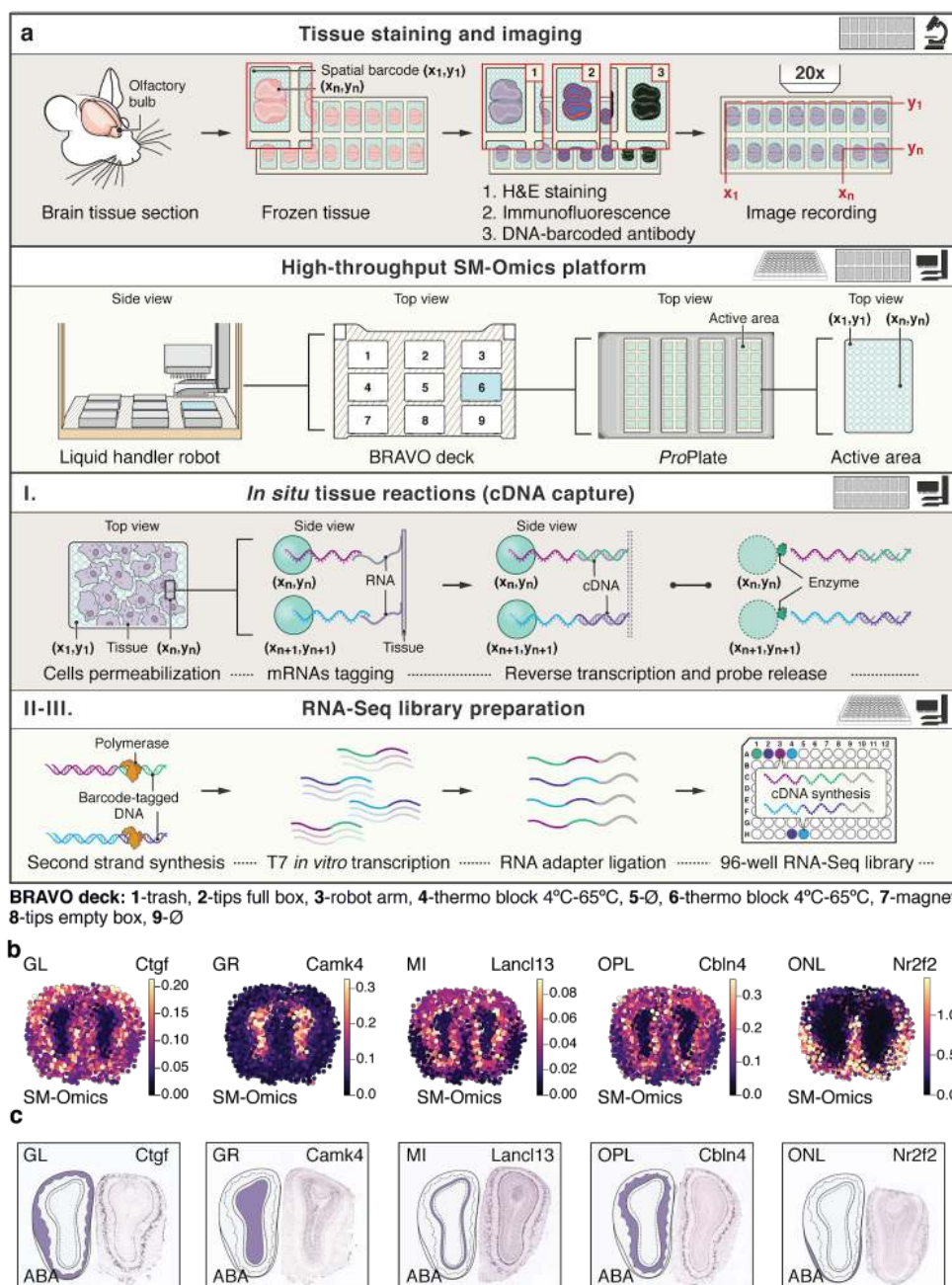
1029
1030 **FigS8. Spatial gene expression specificity and patterns in major annotated layers in SM-Omics and**
1031 **ST** **(a)** Morphological gene expression signatures agree between SM-Omics and the Allen Brain Atlas
1032 (ABA) for the major layers. p-value of Fisher's test (color scale) for the enrichment of genes associated
1033 with each layer in SM-Omics (columns) and in the Allen Brain Atlas (rows). **(b)** Same as in (a) but shown
1034 for ST. Color scale denotes significant p-values ($p \leq 0.05$, Fisher's exact test, one sided, Benjamini-
1035 Hochberg corrected for multiple testing) in panels **(a)** and **(b)**. **(c)** Examples of spatial annotation patterns
1036 (black) for four major morphological regions present in the adult MOB (**Methods**). **(d)** Examples of SM-
1037 Omics spatial gene expression patterns (color scale) for DE genes detected (**Methods**) between the regions
1038 GL, GR, MI and OPL with **(c)** corresponding ISH images from ABA and **(e)** ST spatial gene expression

1039 (color scale) for the same DE genes as in **(f)**. Annotated region abbreviations: GL (Glomerular Layer), GR
1040 (Granular Cell Layer), MI (Mitral Layer) and OPL (Outer Plexiform Layer) are shared between the panels.

1041
1042 **FigS9. Feasibility and quality of combined antibody immunofluorescence and spatial transcriptomics**
1043 **measurements. (a)** Top panel represents cortex region images in the following order: H&E stained, only
1044 DAPI stained, only NeuN stained or DAPI/NeuN stained tissues. Bottom panel shows fluorescent gene
1045 activity as Cy3 cDNA footprints corresponding to top panels. No significant differences were observed in
1046 Cy3 cDNA signal intensities between the conditions (data not shown, Wilcoxon's rank sum test, $p>0.05$).
1047 **(b)** Total number of detected and UMIs per spot under and outside of the tissue boundaries in SM-Omics
1048 when tissue staining was performed with 3 different conditions: H&E (purple, $n=3$), DAPI (blue, $n=3$) and
1049 a combined DAPI and immunofluorescent (IF) stain (red, $n=3$). **(c)** ISH images from ABA for DE genes in
1050 each morphological region (columns). Examples of SM-Omics spatial gene expression patterns (color
1051 scale) for the same DE genes detected (**Methods**). Shown in rows are spatial patterns resulting after 3
1052 different staining conditions as in **(b)**. **(d)** Morphological gene expression signatures agree between SM-
1053 Omics and the ABA for the all major layers present and in all 3 staining conditions. p-value of Fisher's test
1054 (color scale) for the enrichment of genes associated with each layer in SM-Omics (staining conditions in
1055 columns) and in the Allen Brain Atlas (rows). Annotated region abbreviations: CTXSP (Cortical subplate),
1056 HIP (Hippocampal formation), HY (Hypothalamus), TH (Thalamus), CNU (Cerebral nuclei), ISOCTX
1057 (isocortex) and PIR (Piriform area) are shared between the panels.

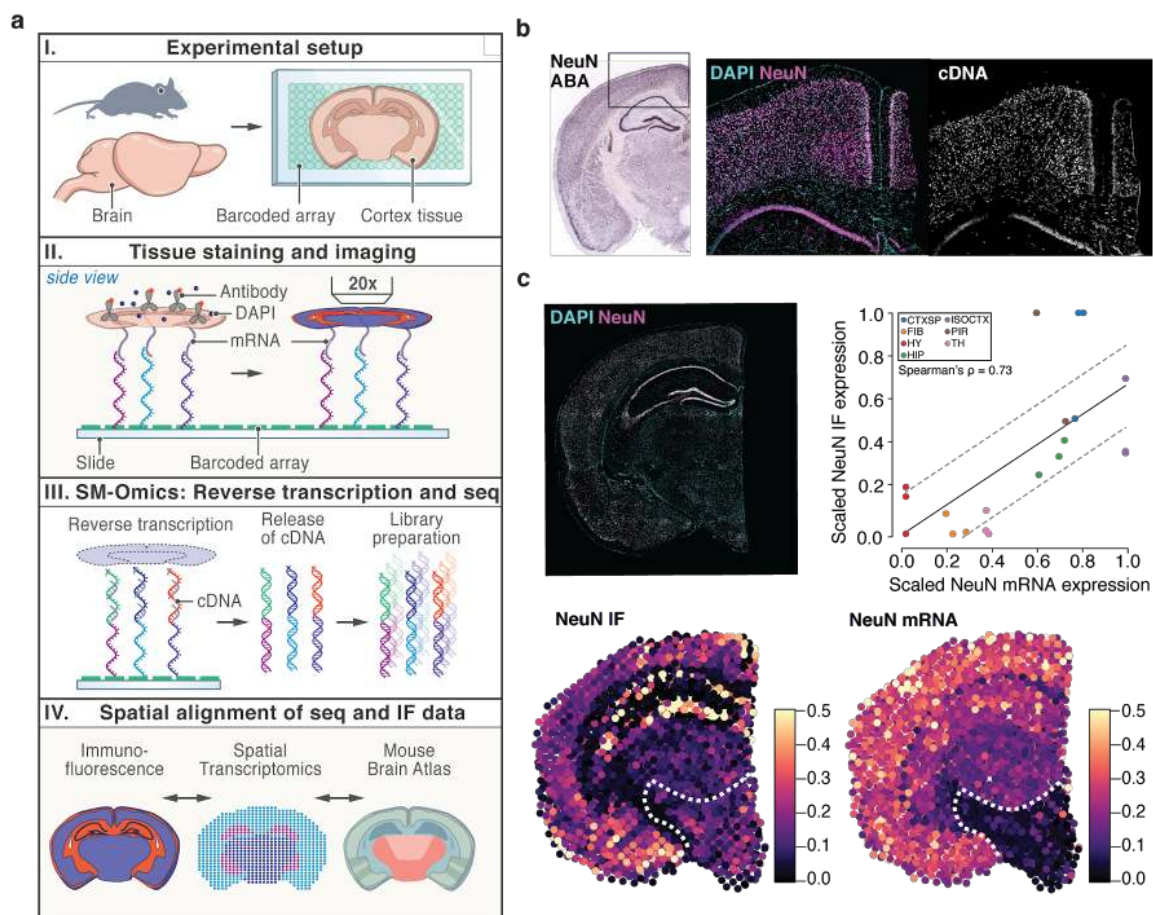
1058
1059 **FigS10. Feasibility and quality of combined antibody immunofluorescence, antibody tags and spatial**
1060 **transcriptomics measurements. (a)** Correlation between scaled antibody tag and respective IF expression
1061 per tissue section ($n=3$, **Methods**) for the two targets: F4/80 and IgD. Denoted is the Spearman's correlation
1062 coefficient (ρ) between moieties. Colored line represents the linear regression line between the conditions
1063 with respective standard deviations (dashed gray lines). Color code represents 4 annotated splenic regions.
1064 **(b)** Correlation between scaled mRNA and respective antibody tag expression per tissue section ($n=3$,
1065 **Methods**). Denoted is the Spearman's correlation coefficient (ρ) between moieties. Colored line (black)
1066 represents the linear regression line between the conditions with respective standard deviations (dashed
1067 gray lines). Color code is shared with **(a)**. **(c)** IF images of 6 antibody clones: F4/80, IgD, CD163, CD38,
1068 CD4 and CD8a.

1069 **Fig1**



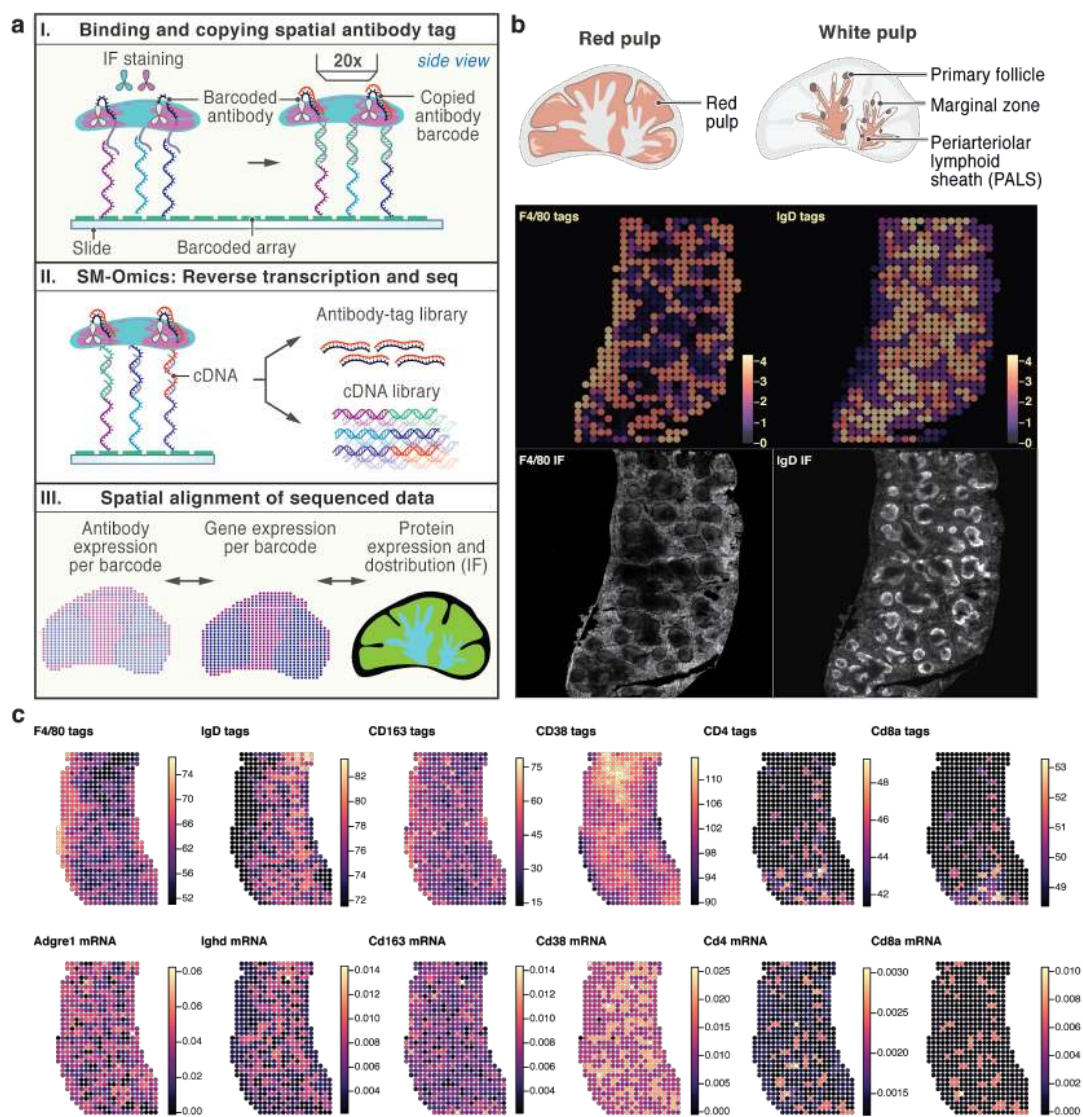
1070

1071 **Fig2**



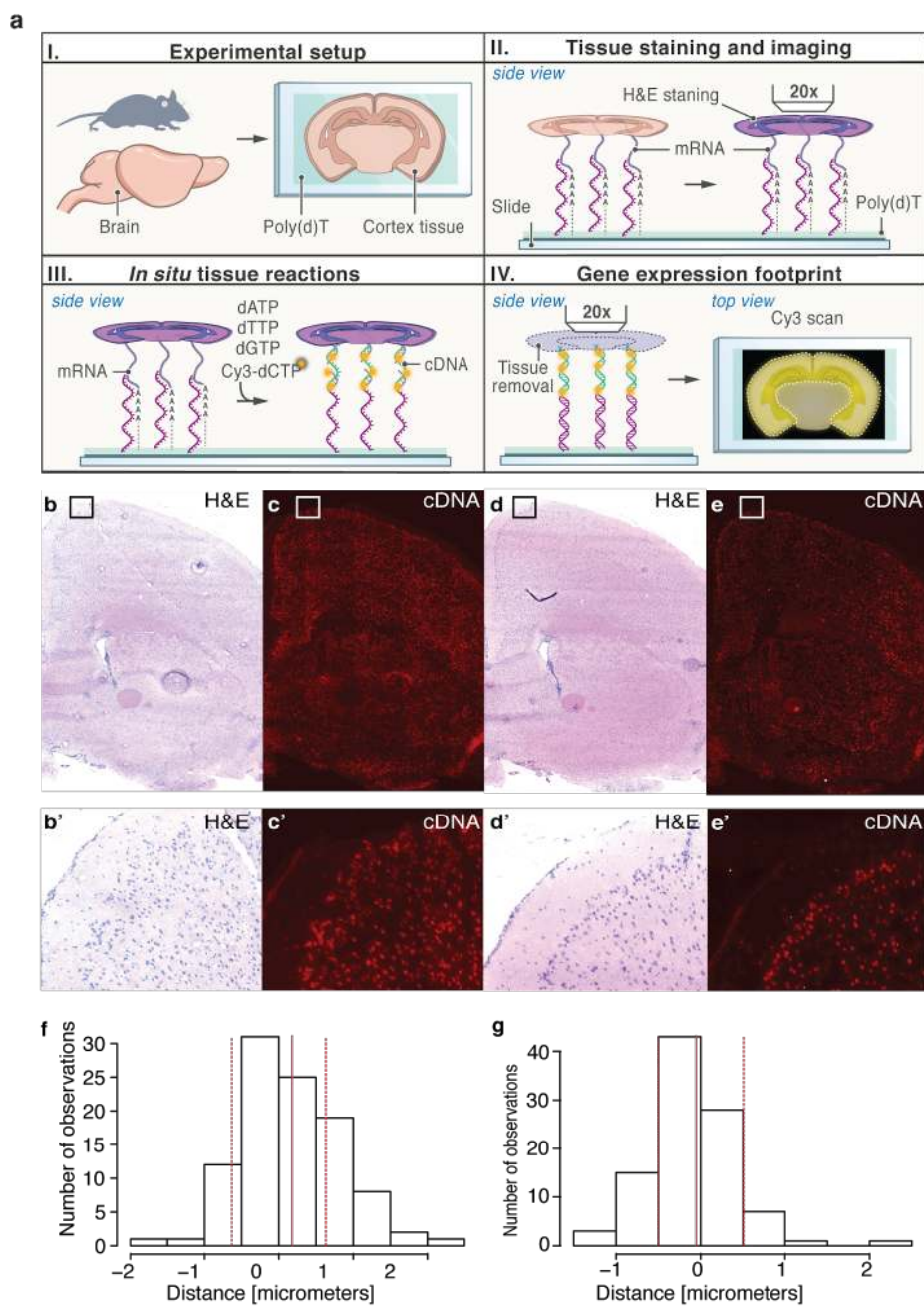
1072
1073

1074 **Fig3**



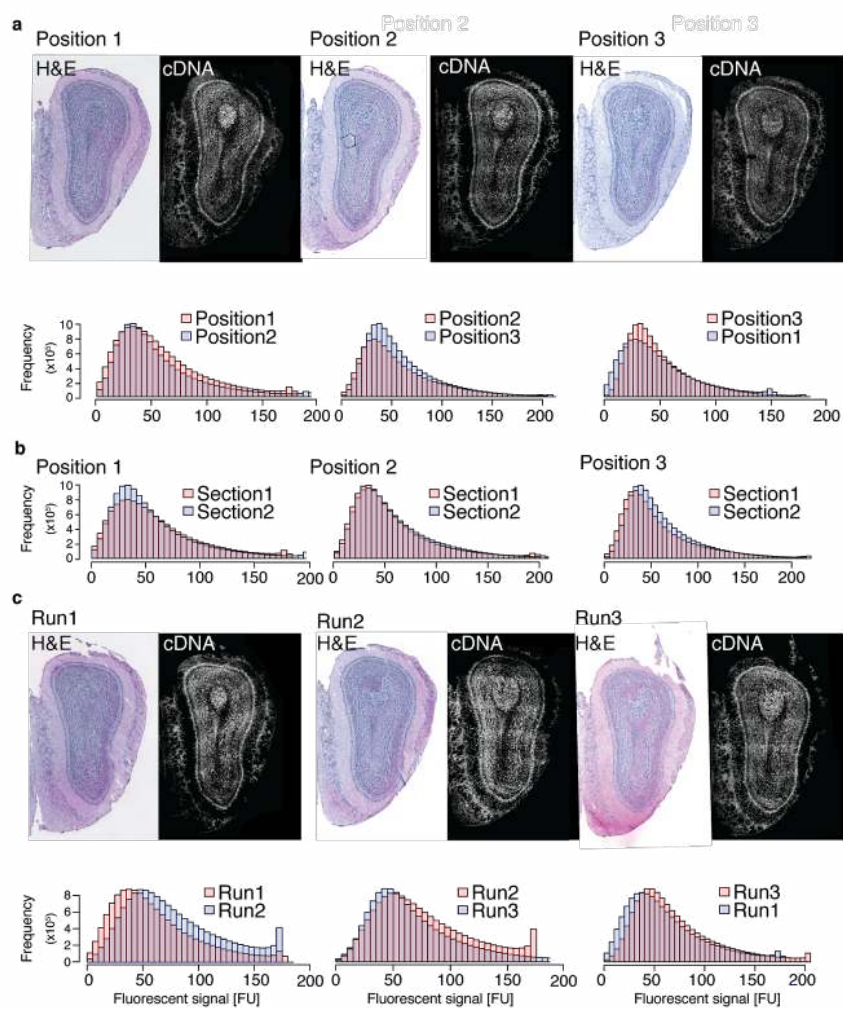
1075
1076

1077 **FigS1**



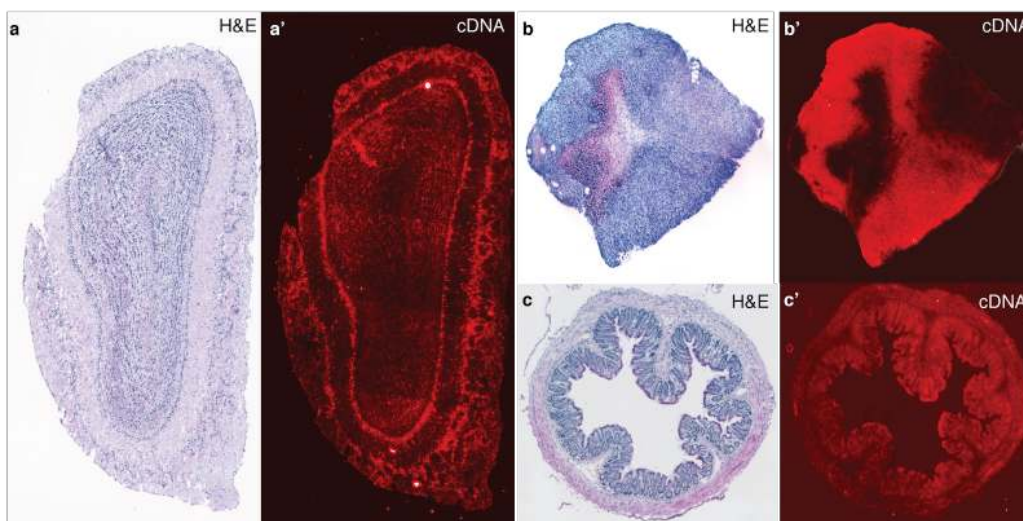
1078

1079 **FigS2**



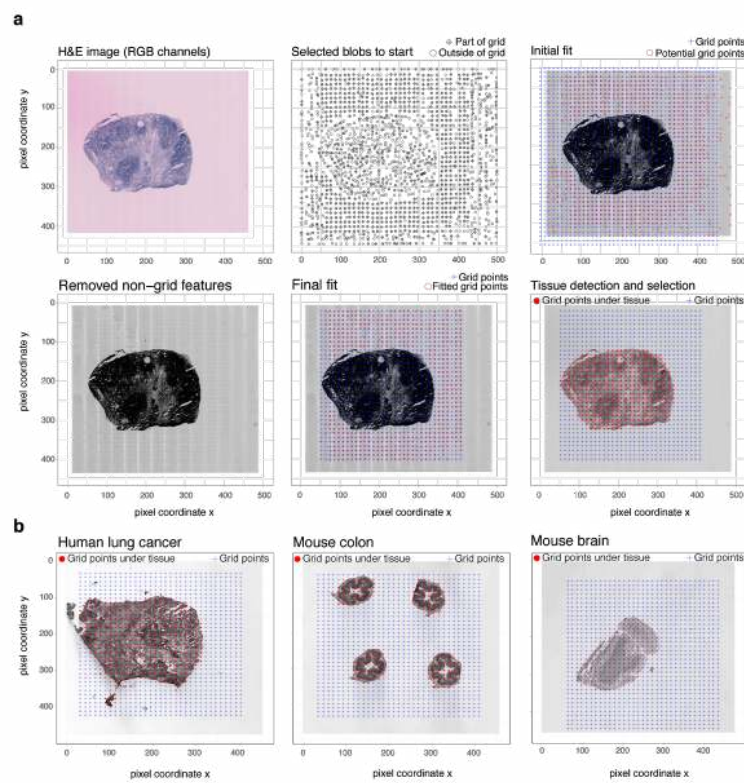
1080
1081
1082

1083 **FigS3**



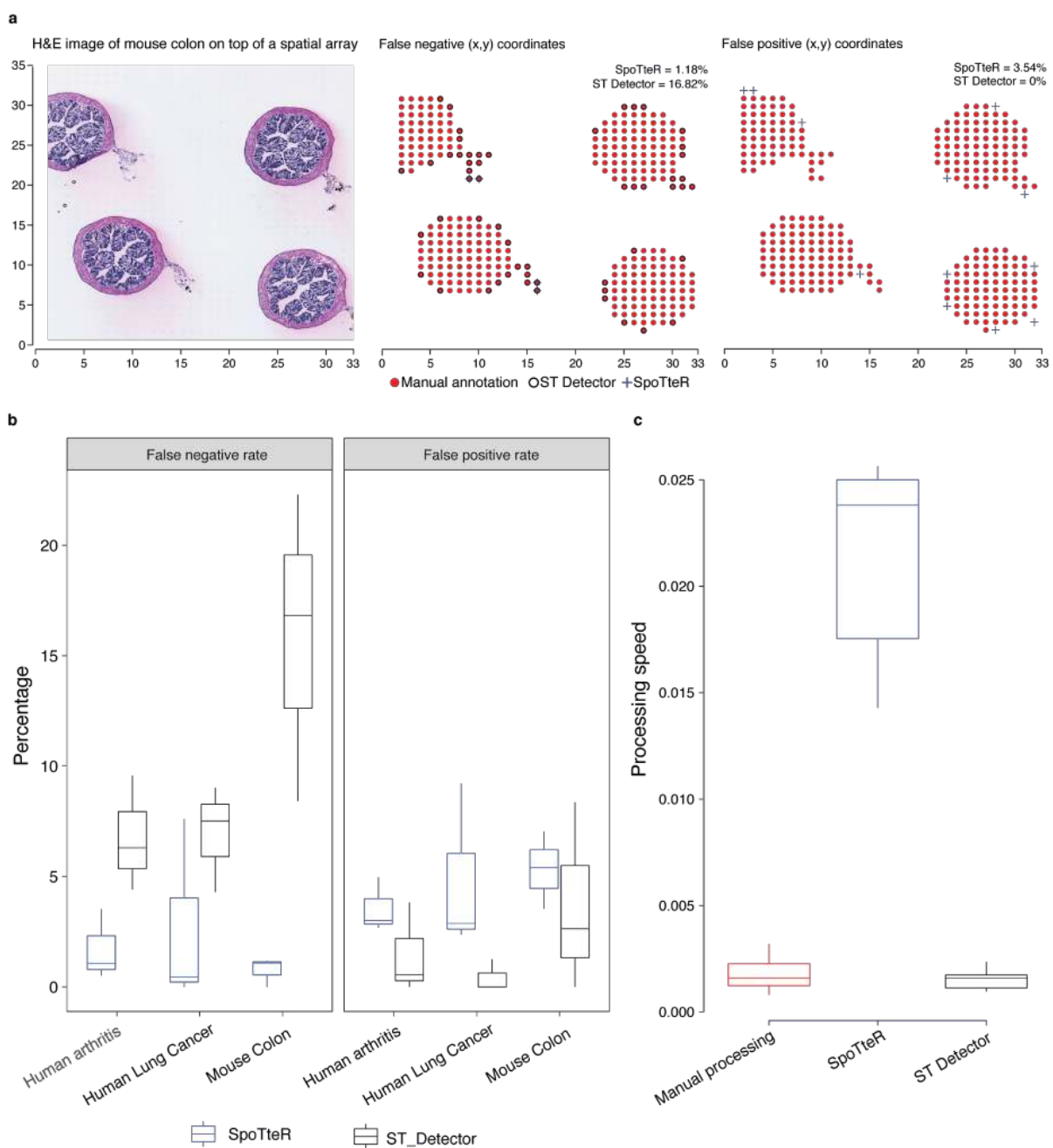
1084

1085 **FigS4**
1086



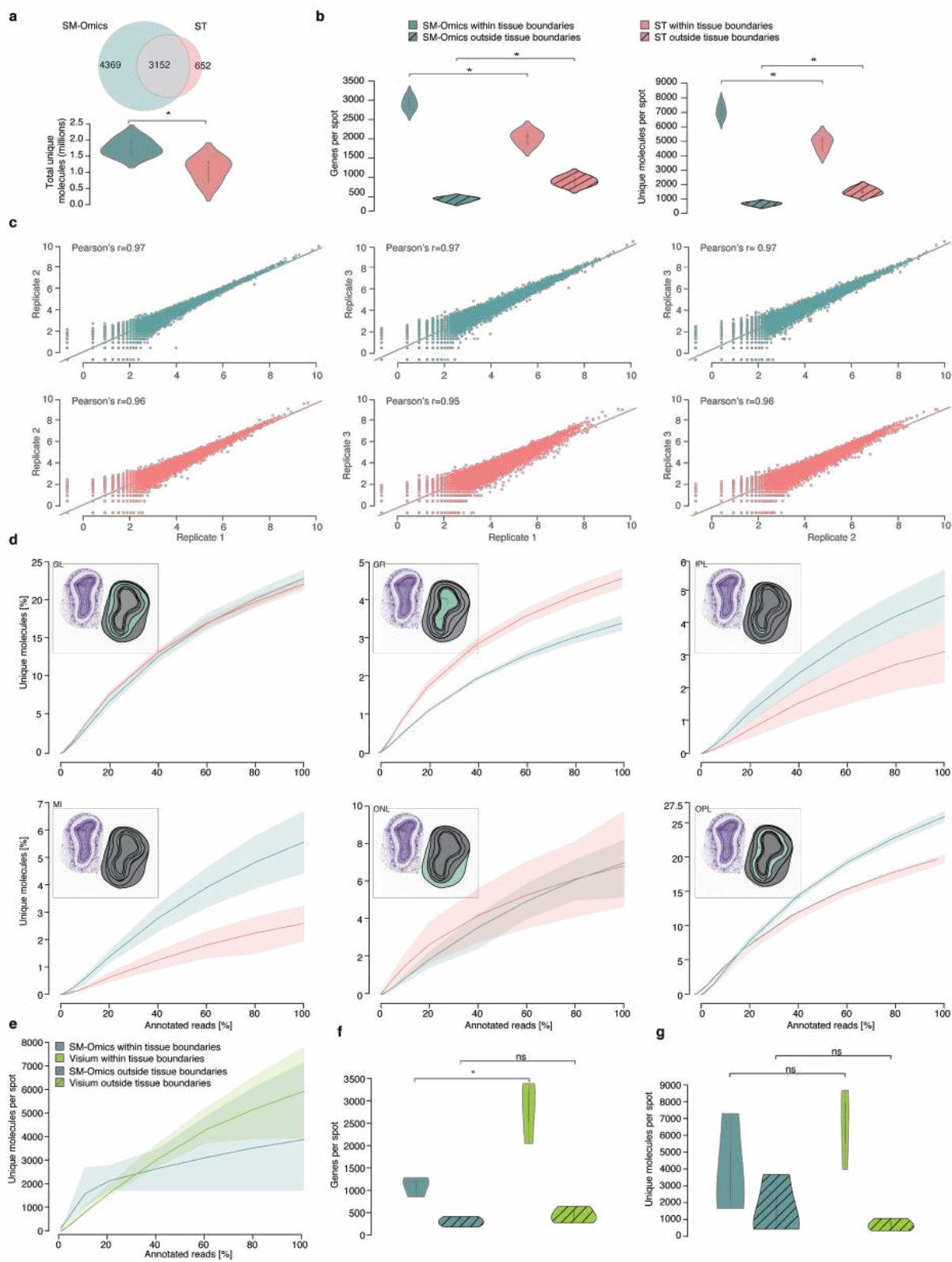
1087

1088 **FigS5**



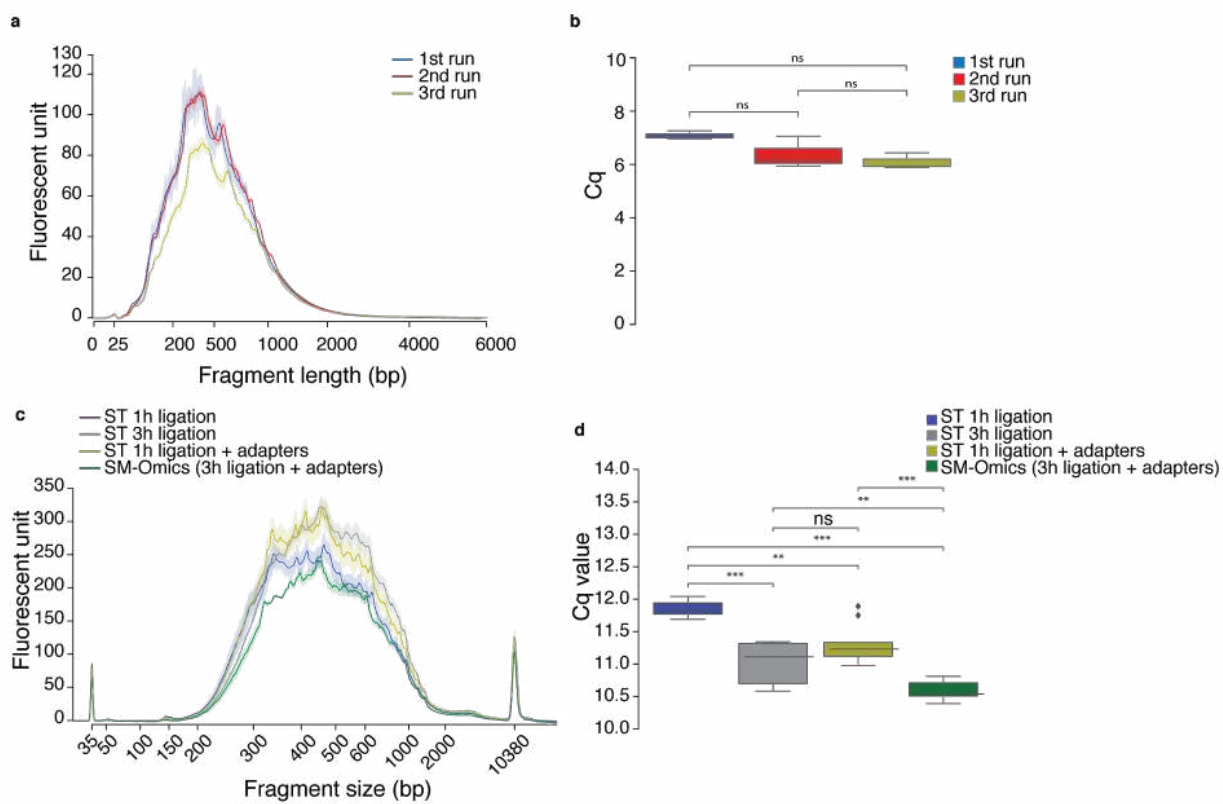
1089
1090

1091 **FigS6**



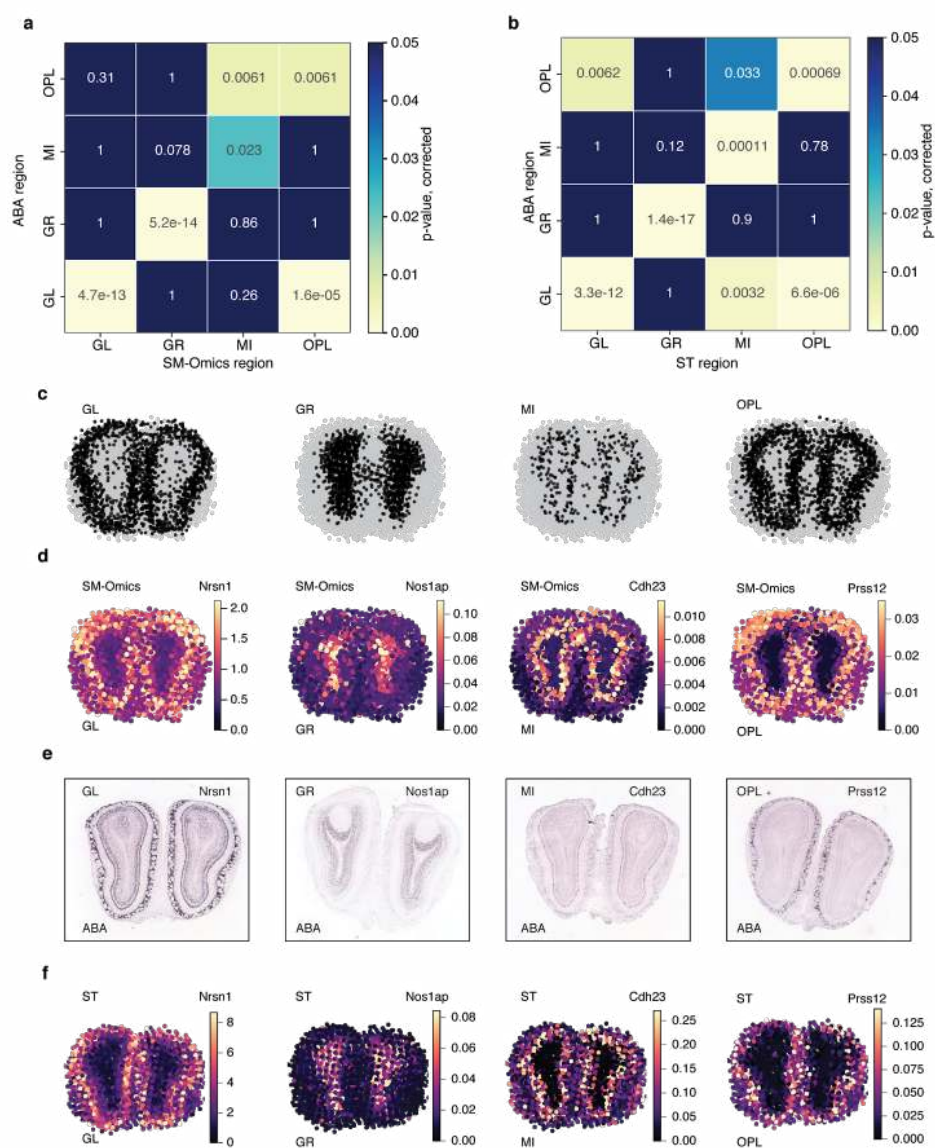
1092

1093 **FigS7**



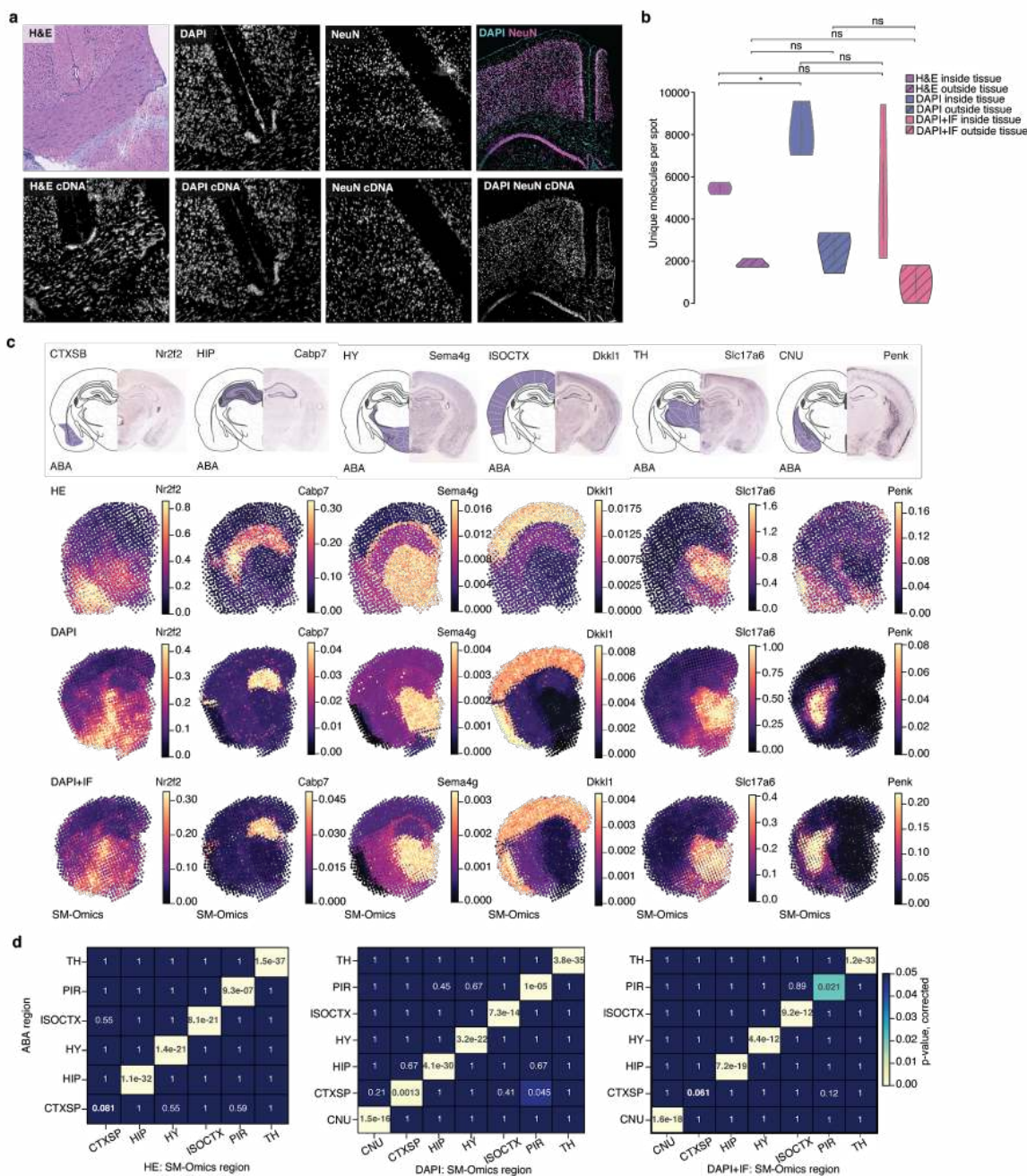
1094

1095 **FigS8**



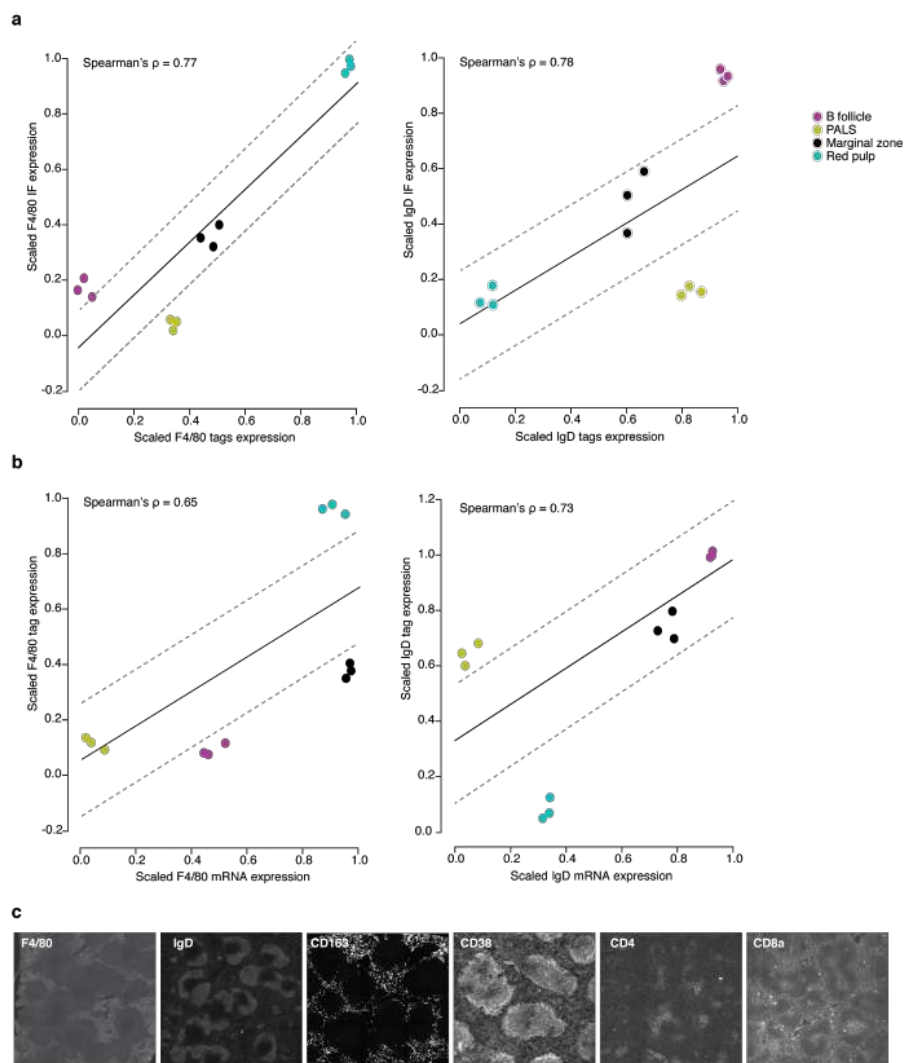
1096
1097

1098 **FigS9**
1099



1100

1101 **FigS10**



1102
1103
1104